New perspectives on radium behavior within a subterranean estuary

Meagan Eagle Gonneea[1], Paul K. Morris[2], Henrieta Dulaiova[1], and Matthew A. Charette[1]

[1]Department of Marine Chemistry and Geochemistry, Woods Hole Oceanographic Institution, Woods Hole, MA, 02543 USA

[2]National Oceanography Centre, University of Southampton, European Way, Southampton, SO14 3ZH UK

Abstract:

Over the past decade, radium isotopes have been frequently applied as tracers of submarine groundwater discharge (SGD). The unique radium signature of SGD is acquired within the subterranean estuary, a mixing zone between fresh groundwater and seawater in coastal aquifers, yet little is known about what controls Ra cycling in this system. The focus of this study was to examine controls on sediment and groundwater radium activities within permeable aquifer sands (Waquoit Bay, MA, USA) through a combination of field and laboratory studies. In the field, a series of sediment cores and corresponding groundwater profiles were collected for analysis of the four radium isotopes, as well as dissolved and sediment associated manganese, iron, and barium. We found that in addition to greater desorption at increasing salinity, radium was also closely tied to manganese and iron redox cycling within these sediments. A series of laboratory adsorption/desorption experiments helped elucidate the importance of 1) contact time between sediment and water, 2) salinity of water in contact with sediment, 3) redox conditions of water in contact with sediment, and 4) the chemical characteristics of sediment on radium adsorption/desorption. We found that these reactions are rapid (on the order of hours), desorption increases with increasing salinity and decreasing pH, and the presence of Fe and Mn (hydr)oxides on the sediment inhibit the release of radium. These sediments have a large capacity to sorb radium from fresh water. Combined with these experimental results, we present evidence from time series groundwater sampling

that within this subterranean estuary there are cyclic periods of Ra accumulation and release controlled by changing salinity and redox conditions.

Keywords: radium; sediments; desorption; adsorption; barium; submarine groundwater discharge; subterranean estuary; redox reactions; ion exchange; distribution coefficient

1. Introduction

The subterranean estuary (STE), as defined by Moore (1999), is an underground chemically reactive zone of mixing between fresh groundwater and seawater that intrudes into the aquifer. Chemical reactions within this zone combined with submarine groundwater discharge (SGD) are known to have a large impact on coastal budgets of various constituents including nutrients, trace metals and radioisotopes (Charette and Sholkovitz, 2002; Windom and Niencheski, 2003; Slomp and van Cappellen, 2004). Many studies have used the unique geochemical signal originating from the subterranean estuary to determine rates of transport of such constituents to the coastal ocean via submarine groundwater discharge (Burnett et al., 2006 and references therein). Examples of SGD tracers are the four naturally occurring radium isotopes (^{223}Ra $t_{1/2}$ = 3.66 d, ^{224}Ra $t_{1/2}$ = 11.4 d, ^{228}Ra $t_{1/2}$ = 5.75 y and ^{226}Ra $t_{1/2}$ = 1,600 y); their use in this approach is based on measuring the excess radium in surface water resulting from SGD, and the radium activity in the groundwater that supplied the excess. The latter parameter usually varies considerably, and is therefore one of the largest sources of uncertainty in Ra-derived SGD rates. To reduce this uncertainty, we require a better understanding of what controls Ra cycling in coastal groundwater systems.

Our perception of how Ra might behave in subterranean estuaries has mostly been derived from studies of their above-ground counterpart. Ra release in surface estuaries has been mainly attributed to desorption of Ra from suspended and bottom sediments as salinity increases (Li and Chan, 1979; Elsinger and Moore, 1980). However, radium behavior within the STE has additional complexity including varying fractions of exchangeable sediment Ra (Porcelli and Swarzenski, 2003); grain size and porosity of sediments (Webster et al., 1995, Hancock et al., 2006); changes in ionic strength (salinity) (Elsinger and Moore, 1980; Webster et al., 1995); temperature effects (Rama

and Moore, 1996); pH (Sanchez and Rodriguez-Alvarez, 1999; Lauria et al., 2004); and barite solubility (Ba and Ra are chemical analogs) (Langmuir and Riese, 1985; Grundl and Cape, 2006). Other controls have been suggested but not thoroughly examined including the redox state of groundwater (including Eh and pH) (Puigdomènech and Bergström, 1995; Porcelli and Swarzenski, 2003) and the presence Fe and, in particular, Mn (hydr)oxides, since Ra has a very high affinity for Mn and Fe (Bollinger and Moore, 1993; Sun and Torgersen, 2001; Charette and Sholkovitz, 2006).

It is well known that sediment redox conditions drive the solubility of Mn and Fe, in particular that Mn and Fe are mobilized when both Eh and pH decrease (Miao et al., 2006). This potential control on Ra desorption has not been thoroughly explored due to the limited data on *in situ* groundwater redox chemistry coupled with groundwater and sediment radium activities. In addition, most laboratory work on Ra adsorption/desorption has not maintained *in situ* redox conditions.

There is also a paucity of *in situ* data on sediment Ra activities and resulting pore water Ra levels. Much of the data on sediment Ra activities are collected from discreet depths from wells and piezometers or consist of depth profiles for surface or shallow (<1 m) sediments. While important geochemical reactions do occur over this depth, there is likely additional complexity that will impact Ra cycling in deeper sediments. Due to the small number of data on Ra activities within STE sediments, particularly saturated sands, from depths greater than one meter, much of the Ra sediment chemistry is based on surface or shallow sediments and scaled to the larger study area.

This study investigates the sediment and groundwater radium distributions within the STE of Waquoit Bay. This system has been extensively studied, with a well established underground mixing zone between fresh groundwater and recirculating seawater occurring over a narrow (~10 m) region (Figure 1), creating an ideal natural laboratory for investigating sediment and groundwater Ra dynamics. Seasonal changes in water table height result in movement of the fresh/salt interface, thus periodically changing the ionic strength and redox conditions of the water saturating sediments. Recharge of the aquifer occurs during the winter and spring, and the fresh/salt interface moves seaward, while during the summer and fall, the aquifer levels drop and sea water intrudes further into the STE (Michael et al., 2005).

In addition, there are active Fe/Mn redox cycles within the Waquoit Bay STE sediments (Charette and Sholkovitz, 2002; Charette et al., 2005). Charette and Sholkovitz (2006) proposed several controls on Ra chemistry, including 1) adsorption onto Fe/Mn (hydr)oxides, 2) desorption from sediments via ion-exchange reactions, 3) release from oxides undergoing reductive dissolution and 4) sediment weathering. Here we report on a series of sediment cores and groundwater profiles which were collected to examine Ra dynamics *in situ*. Additional information about the Fe/Mn redox cycles of the Waquoit Bay STE is presented for sediments deeper in the aquifer (7 m) so we can evaluate how *in situ* redox conditions affect Ra cycling in these sediments. A series of laboratory experiments were then carried out on the sediment to further explore adsorption/desorption reactions rates and sediment partition coefficients (K_d) under varying ionic strength and redox conditions and for sediments of differing Mn and Fe (hydr)oxide content. Finally, a time series of groundwater salinity, Ra, Mn, Fe, pH and Eh was evaluated to see if the laboratory findings were consistent with field measurements.

1.2 Model of sediment Ra partitioning: caveats and considerations

The partitioning of Ra into different fractions within individual sediment grains has important implications for sediment-pore water Ra exchange. The total sediment Ra is commonly termed bulk or total Ra. This includes Ra within the sediment lattice, which is only available for exchange with pore water during sediment weathering, a process which occurs over very long time periods and is usually insignificant compared to other processes. Some fraction of the bulk Ra is termed "surface bound Ra" whether it is bound to an organic coating, siliceous oxide or Mn-Fe (hydr)oxide. This fraction is the focus of this study, since under varying geochemical conditions, different fractions of this pool are available to exchange with adjacent pore waters. The surface bound ^{226}Ra is usually evaluated via the ^{222}Rn-emanation method (Elsinger and Moore, 1980; Corbett et al., 1998), while surface bound ^{224}Ra can be measured by coincidence counting of sediments (Sun and Torgersen, 1998). This study considers the various geochemical controls on Ra exchange between the surface bound Ra pool and groundwater dissolved Ra.

2. Methods

2.1 Study Area

Waquoit Bay is a shallow estuary located along the southern shore of Cape Cod, MA, USA (Figure 1). The upper 10 m of the Cape Cod aquifer consists of fairly homogenous permeable sediments (Cambareri and Eichner, 1998) with a well defined subterranean estuary beneath the shore of Waquoit Bay (Testa et al., 2002; Talbot et al., 2003; Michael et al., 2005). Boreholes drilled through the STE of Waquoit Bay reveal fine to coarse sand (0-10 m) underlain by fine to very fine sand and silt (Cambareri and Eichner, 1998). Grain size analysis of several sand samples from the top 2 m at the head of the bay indicates that the shallow sediment consists of >95% sand and <5% silt and clay (Charette et al., 2005). A microscope screening of sediments by W. Bach (pers. comm.) revealed that the majority of the monomineralic grains are quartz. There is <1% of plagioclase along with traces of clinopyroxene, amphibole, white mica, magnetite and at least one other oxide (goethite or hematite). Polymineralic fragments in the sands probably represent granite, schist, amphibolite and gabbro. Early studies of the sediment geochemistry describe a zone of Fe hydr(oxide) coated sands resulting from the precipitation of oxides from a large Fe plume in the fresh groundwater (Charette and Sholkovitz, 2002). Charette et al. (2005) describe the redox chemistry of Fe, Mn, Ba, U and Th in the upper 2 m of the aquifer.

Numerous studies have documented the importance of submarine groundwater discharge on nutrient and chemical budgets in Waquoit Bay (Valiela, et al., 1990; Charette et al., 2001; Bone et al., 2006). Radium isotopes have been employed to determine the magnitude of SGD (0.035 m^3 s^{-1}, Mulligan and Charette, 2006) and several studies report considerable variability in groundwater radium activities (Charette et al., 2001; Abraham et al., 2003; Gonneea et al., 2006; Mulligan and Charette, 2006).

Samples for this study were collected in June 2006, when aquifer levels were dropping and the fresh/saline groundwater interface was moving landward, inundating sediments that had been exposed to freshwater during the winter recharge period of the aquifer with higher salinity groundwater.

2.2 Field Methods

A series of three sediment cores (down to 7 m) were collected in June 2006 with a hand operated bailer boring auger system (Figure 1). The sediment was collected in the 60 cm long auger which was pushed into the ground and filled with sediment. The recovered sediment was then pulled up to the surface and collected in sample bags. As the auger was removed, a plastic core casing was pushed down the hole to prevent sand from collapsing into the hole. The theoretical sampling resolution is 60 cm, limited by the length of the sediment auger barrel; however, in practice "heaving" sands at depth resulted in sediment from the depth of the bottom of the core casing being pushed up the casing. Sediments pushed up the core casing in this way were assigned a depth corresponding to the bottom of the core casing. A very distinct color stratigraphy associated with different Fe and Mn (hydr)oxide layers was observed in the sediments, which verifies that we successfully sampled distinct sediment depths.

Groundwater samples were collected concurrently with the sediment samples, at a site offset by 1.5 m from the coring site. A hollow stainless steel drive point piezometer system (Retract-a-tip™) capable of a 0.06 m sampling resolution (we sampled every 0.15 m) was used (Charette and Allen, 2006). Water was pumped through a clean nylon tube within the piezometer with a peristaltic pump. Basic water chemistry data including salinity, dissolved oxygen, temperature, pH and ORP (standardized to Eh) was measured with a YSI 600XLM in a flow-through cell (YSI, Inc.) In addition, separate water samples were collected for salinity and were analyzed by a Guideline AutoSal instrument. Samples for trace metals were collected in pre-acidified (2 µL/ml 8 N Optima nitric acid) HDPE containers. Groundwater (4L) was filtered through MnO_2 impregnated acrylic fibers (hereafter Mn fibers) at a flow rate of 0.2 L/minute to quantitatively sorb Ra onto the MnO_2 (Moore and Reid, 1973).

2.3 Laboratory Methods

Sediments were brought back to the laboratory and stored at 4°C prior to analysis. Subsamples from the three sediment cores were dried, packed in 8 cm diameter jars, sealed with epoxy resin and left for > 3 weeks to ensure secular equilibrium between ^{226}Ra and its daughter radionuclides and then counted on planar gamma detectors for bulk

sediment ^{228}Ra (via ^{228}Ac at 338 keV), ^{226}Ra (via ^{214}Pb at 351.9 keV), and ^{238}U (via ^{234}Th at 63.6 keV). The program GESPECOR, a Monte Carlo based software used for calibration of pure Ge detectors, was used to calibrate the detector for the geometry described above (Sima and Arnold, 2002). Grain size was determined with a Beckman Coulter LS13320 laser diffraction particle size analyzer. A portion of each sediment sample was subjected to an operationally defined leach to determine the concentrations of Fe, Mn, Ba and U associated with amorphous and crystalline oxides of Fe and Mn (Hall et al., 1996). Briefly, 0.2 g of sediment was combined with 10 mL of 0.25 M hydroxylamine hydrochloride in 25% glacial acetic acid and heated for 3 hours at 90°, decanted and then the leaching was repeated. An aliquot of the leachate was diluted 1:50 with 1 N Optima grade nitric acid. The resulting solution was analyzed via inductively coupled mass spectrometry on a Finnigan Element high resolution ICP-MS at Woods Hole Oceanographic Institution. Indium (In) was used as an internal standard to account for instrument drift and matrix effects of the solution. Count rates for all elements were normalized to In measured in samples and standards.

The Mn fibers with the groundwater radium isotopes and sediment desorption Ra (Section 2.4) were rinsed with Ra-free water to remove salts which interfere with counting (Sun and Torgersen, 1998), partially dried and placed within a delayed coincidence counter to measure ^{223}Ra and ^{224}Ra (Moore and Arnold, 1996). Samples were then ashed (820°C, 16 h), homogenized and capped with epoxy, as with the sediment samples, prior to being placed within a well-type gamma spectrometer to measure ^{226}Ra and ^{228}Ra (Charette et al., 2001). All detectors were standardized using a NIST-certified Standard Reference Material sorbed to Mn fibers and prepared in the same manner as the samples. Detection limits calculated with the Currie Hypothesis test for these samples were 0.2 dpm (i.e. 0.16 dpm/100 g for desorption experiments with 120 g sediment and 0.05 dpm/L for 4 L groundwater samples) (De Greer, 2004). ^{223}Ra, ^{224}Ra, and ^{228}Ra activities were decay corrected for the time of collection.

Groundwater concentrations of dissolved Fe, Mn, and Ba were measured by ICP-MS as described above for sediment leach samples. Each sample was diluted 1:20 with 1 N Optima nitric acid and spiked with an internal In standard.

2.4 Adsorption/desorption experiments

The amount of exchangeable Ra associated with these sediments was assessed with a series of experiments. Sediment from three depths in PZ 11: 1) 2.1 to 3.1 m (low Mn, intermediate Fe), 2) 4.5 to 5.6 m (intermediate Mn, High Fe) and 3) 5.8 to 6.5 m (high Mn, low Fe), referred to hereafter as the top, middle and bottom of the core respectively, were chosen based on their differing sediment chemistry and resulting coloration (see shaded areas in Figure 1 and Table 1). Groundwater of varying salinity was prepared for these experiments by mixing fresh groundwater with seawater. Fresh groundwater was collected from the Waquoit STE, and saline water was collected from Vineyard Sound, the seawater source to Waquoit Bay and ultimately the STE. The water was filtered (1 μm) to remove the bulk of the particulates and then passed through Mn fibers to ensure the water used was initially free of Ra. The freshwater and seawater was then mixed in varying ratios until the desired salinity was achieved.

For the first experiment, the amount of surface bound ^{226}Ra was determined via radon emanation by equilibrating 100 g of sediment with 500 mL of radium free water at a salinity of 10.8 for 3 weeks (Corbett et al., 1998). The salinity of the water used for this measurement should not impact the results, since Rn will be in equilibrium with any Ra that desorbs from the sediments into the water and the Ra that remains surface bound.

The second experiment was aimed at determining the fraction of surface bound Ra that would desorb from sediment under differing salinities and desorption times. Since this experiment was done with sediments of differing Fe and Mn (hydr)oxide contents, the impact of Fe/Mn sediment chemistry on Ra desorption was also evaluated with this experiment. Multiple, sacrificial replicates of sediment were mixed with water of varying salinities and left for various time periods. Sediment (350 g wet weight) was mixed in cubetainers with 4 L of Ra-free water, either salinity 5, 15 or 25, added to the sediment aliquots and left for 0.5, 2, 5, 10, 24 and 48 h. Additional samples were exposed for 288 and 4150 hours (at salinity 5 and 25 only) to test the time dependence of desorption . The samples were shaken twice, immediately after the water was added and 1 minute before the water was separated from the sediment by decanting it into another container. Decanted water was pumped sequentially through clean acrylic fiber and then Mn fiber at a rate of < 0.4 L min^{-1}. The clean acrylic fiber served as a prefilter to remove

the bulk of fine, suspended particles contained within the decanted sample and the Mn fiber was used to extract all the Ra that had been desorbed into the water. The Mn fiber was then rinsed with Ra-free fresh water to remove any salts from the fiber.

The third experiment was designed to ascertain the total sediment ion exchange capacity for Ra. A purified ^{226}Ra standard (100 dpm) was spiked into 20 mL of Ra-free groundwater with a salinity of 0 or 25 and then dripped through sediment columns filled with ~15 g dry weight of sediment at a flow rate of 6-8 mL/h. The solution was passed over the sediment twice, resulting in a total exposure time of 6 hours. The unsorbed ^{226}Ra was removed from the effluent solution by $BaSO_4$ precipitation (modified from Martin et al., 1995). The barite was sealed in a counting vial with epoxy and equilibrated for 3 weeks to allow for the ingrowth of ^{214}Pb and ^{226}Ra was determined by gamma spectrometry via ^{214}Pb at 351.9 keV.

The last experiment was intended to quantify the role of pH on sediment-water Ra partitioning. Experimental conditions were chosen based on observed ranges in these properties from field data (pH from 5.5 to 8.0, with a corresponding Eh from 440 to 95 mV respectively). For this experiment, 3 g of sediment, which had 3.5 dpm/g ^{226}Ra adsorbed (sediments from the third experiment), was mixed for 12 hours with water of salinity 0, 5 or 25 and pH 5 or 8. This sediment was used to allow us to rapidly determine the impact of pH on desorption using a small amount of sediment. The pH 8 water was buffered with 0.05 M imidazole and the pH 5 water was buffered with 0.1M sodium acetate, then pH was adjusted with either 10 N sodium hydroxide or 3 M hydrochloric acid. We also measured the redox potential of the leachate and at pH 5 it was 425 mV, while at pH 8 it was 340 mV, a smaller range than seen in the groundwater. Thus, this experiment primarily tested the influence of pH on desorption, not Eh. The leachate was decanted from the sediment and ^{226}Ra was analyzed using the barite co-precipitation method technique as described previously.

2.5 Time series data

A series of permanent piezometer wells, similar to the field sampling system used above, was installed in 2004 and has been sampled at monthly intervals (TS in Figure 1). The wells were installed at various depths to capture the extent of the fresh/saline

interface as it rose and fell seasonally. The same suite of samples is collected from these wells as was collected during field sampling of groundwater, including salinity, Eh, pH, trace metals, and radium, with the same methods employed to analyze these samples.

3. Results

The Waquoit Bay STE has a well-defined mixing zone between fresh groundwater and circulating seawater. In our study area, the mixing zone between these two components is narrow, usually occurring over 1-2 m, and rises toward the sediment surface to outcrop at approximately the low-tide line. Thus, landward piezometer profiles have a broad region of fresh groundwater, which becomes progressively shallower in seaward profiles. There are three main salinity zones within theses profiles, 1) the freshwater zone, 2) the salinity transition zone, where mixing between the fresh and saline water causes groundwater salinities to rise sharply from fresh to near 20, and 3) the circulating seawater zone, where salinity is greater than 20.

The redox conditions in the groundwater are closely tied to the salinity, since saline groundwater results from the intrusion of bay water that has passed through organic rich surface sediments. When this water enters the aquifer, the organic matter is consumed by bacteria along the flow path, which depletes dissolved oxygen and leads to reducing conditions. In contrast, the fresh groundwater is relatively less reducing. Thus, increases in salinity related to recirculating seawater correspond to decreases in oxidation-reduction potential (Eh) and increases in pH. The relationship between Eh and pH in this STE is driven by the high buffering capacity of the high pH (7-8) saline water, and the low buffering capacity of the acidic (5-6) fresh water. Thus reducing conditions typically have a higher pH than oxidizing conditions. Some small salinity increases at the top of the groundwater profiles do not correspond to decreases in Eh/increases in pH, likely because the salinity is due to “overtopping” of new bay water from a recent high tide that has not resided in the aquifer long enough to become significantly reducing. Within the three salinity zones described above, redox conditions can be either oxidizing (high Eh, low pH) or reducing (low Eh, high pH) depending on its associated organic matter content and how much time the water has spent within the aquifer.

There are four important redox-controlled zones within the sediment where Fe and Mn (hydr)oxides either accumulate on the sands in substantial levels or Fe and Mn are released to the pore water (Figure 2). 1) The tops of all profiles are oxidizing, with high Eh and low pH values. There is some accumulation of sediment Mn (hydr)oxides (PZ 6 and 7) and Fe (hydr)oxides (PZ 6) within this zone. 2) A reducing zone follows which is associated with a small (1-2) increase in salinity. This zone is marked by a release of Ra, Ba, Mn and Fe from the sediments. 3) A second oxidizing zone follows, which is marked by an accumulation of Fe (hydr)oxides above Mn (hydr)oxides. 4) Finally, associated with the circulating seawater, the reducing zone at the bottom of each profile is marked by a further release of Ra, Ba, Mn and Fe. A more detailed discussion of these phenomena follows.

3.1 Groundwater Chemistry

Three groundwater profiles (~8 m deep) were collected within the Waquoit STE to capture the extent of the mixing zone between fresh and saline water (Figure 1). PZ 7, the most landward, has a salinity of <2 from 1 to 3.5 m, then is fresh until salinity rises sharply to >10 at 7 m at the STZ (salinity transition zone) (Figure 2a). PZ 6 increases to a salinity of 1 at 5.5 to 6.4 m, then quickly becomes salty, reaching a maximum salinity of 21 (Figure 2b). PZ 11, the most seaward, increases to a salinity of 1 from 4.3 to 5.2 m, then increases to maximum salinity of 25 by 7.3 m (Figure 2c, supplementary information Table 1).

Groundwater profiles show several zones of high Ra activity, usually one above the STZ within the predominantly fresh zone and one beginning concurrent with the STZ and continuing on through the saline zone. ^{224}Ra (10 to 506 dpm/100L), ^{223}Ra (0.5 to 30 dpm/100L), ^{226}Ra (6 to 370 dpm/100L) and ^{228}Ra (6-685 dpm/100L) activities within the STE range over two orders of magnitude (Figure 2).

The redox conditions of the groundwater exhibit a strong control on dissolved Mn, Fe, Ba, and Ra (Figure 2). There are two zones of low Eh/high pH in each profile, an upper zone, 1-2 m thick located between 1 and 4 m depth associated with a plume of high dissolved Fe, and a lower one at the salinity transition zone in each profile. In all profiles, concurrent zones of low Eh/high pH and increased salinity are marked by

increases in dissolved Ba, Mn, Fe and Ra, although the magnitude of increase in Ra is not always the same across all isotopes. For example, at 2 m in PZ 11, salinity rises to 1, Eh decreases, pH increases, groundwater Ba increases from 15 to 300 nmol/kg, Mn from 0.2 to 6.9 μmol/kg, Fe from 0.9 to 177 μmol/kg and ^{228}Ra from 18 to 120 dpm/100L. ^{224}Ra (10 to120 dpm/100L) and ^{223}Ra (0.5 to 6.8 dpm/100L) also display peaks, but the ^{226}Ra increase is much less pronounced (7 to 14 dpm/100L) (Figure 2c). There is a similar pattern at 1.5 m in PZ 6 (Figure 2b). This divergence in profiles between the different isotopes is likely due to the much longer half life of ^{226}Ra resulting in a much longer regeneration time in the sediment Charette et al. (2003).

3.2 Sediment Chemistry

Three sediment cores (5.5 to 7 m deep) were collected concurrently with the groundwater profiles. There is no discernable pattern in the bulk sediment ^{228}Ra (47 ± 12 dpm/100g) or ^{226}Ra (39 ± 6 dpm/100g) profiles. The ^{228}Ra/^{226}Ra for all sediments ranges from 0.7 to 1.7, with an average of 1.2 (supplementary information, Table 2). Sediment-bound Mn (hydr)oxides have a distinct maximum at the bottom of each profile, peaking at >2000 μmol/kg in PZ 6 (7 m) and PZ 11 (6 m) and around 1000 μmol/kg in PZ 7 (5m) (Figure 2, supplementary information Table 2). Sedimentary adsorbed Fe profiles are similar to Mn, however the Fe peak is above the Mn peak and is 25,000 to 30,000 μmol/kg in PZ 6 (5 m) and PZ 11 (5 m) and around 100,000 μmol/kg in PZ 7 (5 m). This Fe-rich zone was described as an "iron curtain" by Charette and Sholkovitz (2002), since it was shown to inhibit the transport into surface water of certain groundwater constituents (i.e. phosphate). The Mn (hydr)oxide-rich zone or "manganese curtain" likely serves as a barrier to the transport of certain elements, including Ba and Ra, which have a high affinity for Mn (hydr)oxides (40 times greater than Fe (hydr)oxides, Moore and Reid, 1973). Adsorbed Ba ranges from 0.5 to 80 μmol/kg and displays a distinct peak (2-8 μmol/kg) concurrent with the Mn curtain. Within the Mn (hydr)oxide-rich zone, there is a linear relationship between sediment Mn and Ba, however no such relationship exists between sedimentary Fe and Ba. There is little variation in grain size (average 550 microns) or dry bulk density (2.6 g/cm^3) for sediments from any of the profiles. Porosity could not be determined directly on these sediments because the manner of collection

disturbed *in situ* conditions, so a published value of 25% was used (Cambareri and Eichner, 1998).

3.3 Desorption/Adsorption Experiments

For many of the processes that control Ra adsorption/desorption, it is useful to consider a model of a sediment grain with two fractions of Ra: a surface bound exchangeable fraction and lattice bound Ra. Of primary interest is the exchangeable fraction of the surface bound Ra pool, since Ra locked within the sediment lattice cannot drive pore water Ra activities on short time scales, particularly when coarse-grained sediments are present. These adsorption/desorption experiments were designed to quantify the relative importance of a variety of parameters for Ra adsorption/desorption between surface bound Ra on sediments and groundwater in contact with these sediments including 1) length of exposure of sediments with water; 2) salinity of groundwater in contact with sediment; 3) pH of water in contact with sediments; 4) the presence of oxidized Mn and Fe precipitated on sediment; and 5) surface bound Ra on sediment. Temperature, another variable that affects Ra desorption (Rama and Moore, 1996), was held constant at 17 ± 0.8 C. These experiments were conducted with sediments from 1) the top of PZ 11 (inundated with freshwater, low sediment Mn and intermediate Fe), 2) middle of PZ 11 (inundated with water of salinity 1-5, within the "Fe curtain" with intermediate sediment Mn and high Fe) and 3) bottom of PZ 11 (inundated with water of salinity 17-23, within the "Mn curtain" with high sediment Mn and low Fe) (Table 1).

3.3.1 Surface bound radium

The amount of surface bound ^{226}Ra was determined via radon emanation and ranged from 6-32 dpm/100g ^{226}Ra (20 to 70% of total ^{226}Ra) with considerably more surface bound ^{226}Ra present at the bottom of PZ 11, within the "Mn curtain", than elsewhere (Figure 2c, Table 1).

3.3.2 Ra desorption and length of exposure

To determine the time dependence of Ra desorption, sediments were exposed to salinity 5 or 25 water for 0.2, 0.5, 1.5, 2.7, 5.2, 10, 25, 290 and 4150 hours. Samples at

salinity 5 were run in duplicate and samples at salinity 25 in triplicate to evaluate natural variability, which is greater than analytical error. We looked at the slope of Ra desorbed versus hours of exposure and then performed a student t-test to look at the variance among two time periods, 0-25 and 200-4000 hours. There is no statistical difference (p value <0.05) between any of the time periods for ^{226}Ra (0.58 ± 0.14 dpm/100g at salinity 5 and 0. 62 ± 0.14 dpm/100g at salinity 25) or ^{228}Ra but ^{223}Ra and ^{224}Ra both increase with time.

Since samples were run in either duplicate or triplicate, we were able to determine the variability inherent in these desorption experiments. To do this, we compiled the standard deviation between duplicate or triplicate samples for each time point at each salinity. On average, the variance for ^{224}Ra is 15%, ^{223}Ra 22%, ^{226}Ra 25% and ^{228}Ra 12% (with analytical error for these samples averaging: ^{224}Ra 4%, ^{223}Ra 16%, ^{226}Ra 10% and ^{228}Ra 6%). Given the large variance between duplicates/triplicates combined with the small increase in Ra desorbed over time, time of exposure (up to ~6 months) has minimal impact on the amount of Ra desorbed, even for the short-lived isotopes which do display some increase with time. This result may be due in part to the experiment set-up, since after the water and sediment were mixed, no further shaking occurred until immediately prior to separating the water from the sediment. Thus, after the radium distribution between pore water and sediments reached equilibrium, it was radium diffusion from the pores to the overlying water that governed the radium concentration in the overlying water, as occurs in the natural environment.

3.3.3 Ra desorption and salinity of groundwater

The effect of salinity on desorption was evaluated by exposing sediment to groundwater with a nominal salinity of 5, 15 or 25 for up to 48 hours (Table 2, Figure 3). As expected, there is an increase in the amount of ^{228}Ra and ^{226}Ra desorbed at increasing salinities from 5 to 25 for all sediments (Table 2). Sediments from the top of PZ 11, with intermediate Fe and low Mn, desorbed 4 to 9 dpm/100g ^{228}Ra, a significantly greater amount than the other sediments (0.3 to 1.2 dpm/100g) (Figure 3d-f). ^{226}Ra displayed the opposite trend, with sediments from the bottom of PZ 11 desorbing 1 to 2.7 dpm/100g, with all other sediments desorbing 0.3 to 0.6 dpm/100g (Figure 3a-c). There are large

ranges in the increase in desorption from salinity 5 to 25 (from 17 to 131%), but it is still apparent that increases in salinity result in increased radium desorption as has been previously observed (Elsinger and Moore, 1980; Webster et al., 1995). For an increase in salinity from 5 to 25, Ra desorption increased around 50%, a value that may be applicable for other settings with permeable siliceous sands. It is encouraging that this value agrees with that of Webster et al. (1995), who reported a range from 0 to 66% increase in desorption between the same salinities for all four isotopes for sediment with a similar grain size from the Bega River.

3.3.4 Ra desorption and sediment chemistry

The sediments used for the desorption experiments were chosen based on their differing surface bound ^{226}Ra activities and Mn and Fe (hydr)oxide content (Table 1). In order to compare desorption from different sediments, we averaged the total Ra desorbed from all time points up to 48 hours for each isotope at each salinity (Table 2). There are several striking features of the desorption pattern of the different isotopes. The first is that sediments from the top desorb six times more ^{228}Ra (4.8-6.9 dpm/100g, Figure 3d) than sediments from the middle (0.35-0.81 dpm/100g, Fe curtain, Figure 3e) and bottom (0.41-0.74 dpm/100 g, Mn curtain, Figure 3f) of PZ 11. Sediments from the top were from the freshwater portion of the aquifer (at least at the time of collection), within the zone of high groundwater ^{228}Ra/^{226}Ra ratios, and had not been exposed to saline water recently. We thus expected the surface bound Ra inventory to be greater than sediments exposed to saline water. Additionally, ^{228}Ra/^{226}Ra activity ratios are higher due to the faster regeneration of ^{228}Ra.

^{226}Ra does not follow the same trend, with four times more desorbing from sediments in the "Mn curtain" at the bottom of PZ 11 (2500 μmol/kg Mn and 43,000 μmol/kg Fe, Figure 3c). The top (45 μmol/kg Mn and 8,700 μmol/kg Fe) and middle (Fe-curtain, 1170 μmol/kg Mn and 43,000 μmol/kg Fe) of PZ 11 had very similar surface bound ^{226}Ra activities (6-10 dpm/100g), while the bottom (Mn-curtain) sediment from PZ 11 had three times more exchangeable ^{226}Ra (32 dpm/100g). Thus it appears, as expected, the presence of Mn (hydr)oxides is an important factor determining the total exchangeable Ra. Fe (hydr)oxides also likely play a role in sedimentary Ra dynamics at

this location. Even though Ra has a 40 times lower affinity for Fe (hydr)oxides than Mn (hydr)oxides (Moore and Reid, 1973), sedimentary Fe is generally more abundant in these sediments than Mn. The Fe/Mn molar ratio for the top sediments is ~300 and for the "Fe curtain" is ~40, while within the "Mn curtain" it is ~3.5.

3.3.5 Ra release and groundwater pH

Ra release is greater at low (5) pH than high (8) pH across salinity 0, 5 and 25. Sediments from the top (intermediate Fe and low Mn) and middle (intermediate sediment Mn and high Fe) release 30 to 70% of the adsorbed Ra, while sediments from the bottom (high sediment Mn and low Fe) release 15 to 45% (Figure 4). Once again, the sediment chemistry influences the amount of Ra release, with sediments from the bottom Mn (hydr)oxide rich layer releasing less Ra than sediments from the top and middle. It is likely that this increased release at pH 5 compared to pH 8 is not only due to desorption, but rather to dissolution of the oxides onto which surface Ra is bound, which explains why Ra release is observed at salinity 0, where significant Ra desorption is not expected (Lauria et al., 2004; Sanchez and Rodriguez-Alvarez, 1999).

3.3.6 ^{226}Ra adsorption

Ion exchangeable Ra was evaluated by passing 20 mL of groundwater spiked with ^{226}Ra through columns filled with separate aliquots of the same sediment used in the desorption experiments above. The results indicate that these sediments have a very large capacity to sorb ^{226}Ra, up to 390 dpm/100g (Figure 5), when compared with in situ adsorbed Ra, which ranges from 6 to 32 dpm/100 g. Since the K_d of radium is known to decrease with increasing ionic strength, we predicted that much more ^{226}Ra would adsorb onto sediments at 0 salinity than at 25 salinity. This is indeed the case, with three times more radium adsorbing onto sediments at salinity 0 compared to salinity 25 (360 compared to 110 dpm/100g, Figure 5). This adsorption plateaus at salinity 15.

3.3.7 Ra dynamics within the subterranean estuary: insight from a time series study

To further evaluate the influence of redox conditions and salinity increases on radium within the STE, we looked at a time series of salinity, Eh, pH, radium and metal

concentrations at two depths within the STE. The advantage of this approach is that we are able to evaluate the influence of changing salinity and redox conditions on a fixed horizon of sediment within the aquifer. At 3.4 m, baseline salinity is <0.5, with episodic increases greater than 2 on several occasions (Figure 6). At 4.7 m, baseline salinity is 25, with a decrease in salinity observed once. There are two release events of ^{226}Ra (not including the high values at the beginning and end of the time series), most visible at 3.4 m, where activities in the groundwater increase from a baseline of 4 dpm/100L to 80 to 170 dpm/100L. The first release event, between 8/05 and 11/05, is associated with an increase in salinity at 3.4 m to ~2. There is no associated decrease in Eh, and no release of Mn, although there is release of Ba, from 300 to 2240 nmol/L. The second release event, between 5/06 and 6/06, is associated with a rise in salinity at both depths and a decrease in Eh, which does not occur, however, until the second month of Ra release. There is a release of Mn at both depths and a release of Ba at 3.4 m. The Ra release at depth is much smaller since these sediments are continually inundated with saline water. The release of ^{226}Ra at 3.4 m in 5/06 is about twice as great (170 dpm/100L) as the one observed between 8/05 and 11/05 (80 dpm/100L), yet the salinity increase at this time was less (1 rather than 2). While not conclusive, this suggests that the reducing conditions associated with the second Ra release play an important part in the magnitude of the release. These data provide *in situ* evidence that redox conditions are as important in Ra cycling as changes in groundwater salinity.

4.0 Discussion

4.1 Ra desorption and groundwater and sediment chemistry

Within this STE, Ra cycling is controlled by a complex interplay of changing salinity and redox conditions. Ra release occurs during both ion exchange and reductive dissolution of Fe-Mn (hydr)oxides. There is evidence for release during ion exchange at the beginning of the salinity transition zone in PZ 6 (Figure 2b) and PZ 11 (Figure 2c) where there is an increase in Ba and Ra (all isotopes) in a highly oxidizing zone (4 m PZ 11, 5 m PZ 6). There is no concurrent increase in dissolved Mn or Fe, as is observed in the reducing zone. Thus, the release of Ba is linked to Ra cycling when both ion exchange and redox conditions affect desorption, while release of Mn and Fe concurrent

with Ra release only occurs under reducing conditions. This pattern suggests that surface bound exchangeable Ra (and Ba) throughout the STE is weakly bound to sediments except in the presence of Mn and Fe (hydr)oxides. Thus, the presence or absence of redox sensitive elements may provide insight into the mechanisms controlling radium adsorption/desorption within other subterranean estuaries.

Further complexity in the STE cycling of Ra is seen in the surface bound enrichment of ^{228}Ra and ^{226}Ra. There is more surface bound ^{226}Ra in the bottom sediments ($^{228}Ra_{Total}/^{226}Ra_{Total}$ is 0.90) compared to the upper sediments ($^{228}Ra_{Total}/^{226}Ra_{Total}$ is 1.66), where surface bound ^{228}Ra is much greater than ^{226}Ra (based on the much greater activity of ^{228}Ra desorbing from these sediments in the desorption experiments). This pattern is also observed in the ^{228}Ra/^{226}Ra ratio of the groundwater, which decreases with depth from 9 to 1. Aquifer sediments generally have ^{228}Ra/^{226}Ra ratios from 0.3 to 1.25 (Tricca et al., 2001; Porcelli and Swarzenski, 2003). Ratios higher than this, as observed here both in the sediment and groundwater ^{228}Ra/^{226}Ra ratios, are evidence of cyclic adsorption and desorption of surface bound Ra. It is likely that there is removal of ^{226}Ra, which has a much longer half-life than the other isotopes, from the upper 2 m of sediment, where there is increased flow (Gonneea et al., 2006). In addition, sediments in the upper part of the STE are rarely inundated with freshwater, thus are expected to have a large amount of surface bound Ra. The sediments at depth, where the surface bound ^{226}Ra is greatest, are within the "Mn-curtain" and are continually inundated with circulating seawater. It is possible that this Mn-coated sand deposit is quite old, and thus ^{228}Ra is significantly depleted through decay processes only.

As expected, upon exposing the sediments to water, equilibrium between sorbed and dissolved radium is established with the dissolved state highly favored as ionic strength increases (high salinity~low sorption). Greater release is seen at low pH (5) compared to high pH (8). As apparent from the long-lived radium results, the kinetics of this equilibrium are fast, on the order of minutes, as has been found elsewhere (Figure 3) (Langmuir and Riese, 1985; Koulouris 1995). In case of the short-lived isotopes, radium is continuously regenerated via the radioactive decay of its insoluble thorium parent leading to a transient increase over time in proportion to its respective production/decay term. For the long-lived radium there is no new radium produced on the time scale of our

experiments; hence only very minor temporal changes occurred in the dissolved radium concentration.

4.2 Cyclic accumulation and release of radium within the STE

Charette and Sholkovitz (2006) proposed a "slow weathering" hypothesis to explain the apparent continued input of Ba and Ra within the STE. They stated: "In contrast with the surface estuary, which continually receives "new" Ba through the transport of suspended particles, the particles that comprise a subterranean estuary are essentially static…thus, in a scenario where the sea level and aquifer recharge is relatively constant (hence, a relatively constant location of the groundwater-seawater mixing zone on decadal time scales), one would expect the desorptive input of Ba (and other alkaline earth elements) to be minimized. Only through the exposure of newly ion exchangeable Ba via slow weathering of aquifer minerals could this non-conservative release of Ba be maintained." Our final time point from the desorption experiment was meant to test this hypothesis. Regardless of salinity, there is no measurable increase in the amount of ^{226}Ra released from the sediment over ~6 months. Hence, we must invoke an alternative mechanism for explaining the apparent sustained input of Ba and long-lived Ra isotopes from STEs into coastal waters over time.

The seasonal shift in Ra derived from SGD as reported by Kelly and Moran (2002) and Charette (2007) requires an annually renewable source of Ra within the STE. The long time scale (~6 month) desorption experiments reported here show that slow weathering cannot account for such an accumulation of Ra in coastal groundwater and subsequent flux to surface water via SGD. However, we suggest that it is possible for sediments within the STE to act as a large ion exchange reservoir, whereby Ra is accumulated and released during wet and dry periods, respectively.

As shown here with adsorption experiments, alumniosilicate sediments have a large capacity to sorb Ra, particularly in fresh water. In addition, field data reveal large releases of Ra to the pore water during periods of landward seawater intrusion into the STE. To determine if enough radium can accumulate on these sediments to account for the observed desorption events, we turned to our time series radium data and calculated the radium balance between two low salinity periods (when Ra may sorb to sediment,

175 days from 1/05 to 7/05 and 135 days from 12/05 to 4/06) and Ra release concurrent with higher salinities (85 days from 8/05 to 10/05 and 70 days from 5/06 to 7/06). In our calculation, we assumed a sediment "box" of 10 cm^3 and a groundwater flow rate of 10 cm d^{-1} (Mulligan and Charette, 2006). Such a box would have a 1-day residence time and a groundwater volume of 0.25 L (based on porosity of 0.25). If the inflowing fresh water has 0.1-0.3 dpm/L ^{226}Ra (Charette, unpublished data), then during the sorption period from 1/05 to 7/05, the sediment box has the potential to sorb 4.5 to 13 dpm ^{226}Ra. From 8/05 to 10/05, brackish groundwater entered the sediment box and released 13 dpm ^{226}Ra to the pore water. Similarly, from 12/05 to 4/06, 3.5 to 10 dpm ^{226}Ra was added to the sediment system, followed by a two month release period that amounts to 17 dpm ^{226}Ra. Though a perfect mass balance was not achieved (a likely artifact of using data from a single depth rather than the entire sediment column/STE), such a sorption/release mechanism could account for most if not all of the seasonal releases of radium from STEs into coastal waters (Bollinger and Moore, 1993; Moore, 1997; Kelly and Moran, 2002; Shellenbarger et al., 2006; Charette, 2007).

Moore (1997) hypothesized that a similar process was at work for the Ganges-Brahmaputra River delta. He suggested that during high river flow periods, the coastal aquifer within the delta region is recharged with freshwater, which loses its radium via sorption to sediments. Then, during low flow periods, saline water is allowed to enter the estuary and intrude into the river delta aquifer, where Ra is released via ion exchange driven desorption. This Ra-enriched fluid would then be carried to the coastal sea via SGD. While the overall mechanisms of Ra uptake/release are the same, the Waquoit STE is different in that the seasonal changes in aquifer height drive movement of the fresh/saline interface, a process that is independent of the salinity condition within the bay.

4.3 Distribution coefficients

The distribution of radionuclides, including Ra, between sediment and water can be quantified using the distribution coefficient (K_d), which is defined here as the ratio of Ra in the solid phase (dpm/Kg) to Ra in the liquid phase (dpm/L) in equilibrium with this sediment and has units of L/Kg.

1) $K_d = Ra_{solid}/Ra_{liquid}$

Distribution coefficients are determined in a variety of ways, usually in laboratory experiments where Ra isotopes are spiked onto sediment/water slurries (Rama and Moore, 1996; Hancock et al., 2006) or in laboratory experiments where sediment and water are equilibrated (Webster et al., 1995). In these cases, K_d may not provide insight as to the mechanisms of adsorption. The assumption that thermodynamic equilibrium has been achieved is not valid for most *in situ* field conditions, since these systems are dynamic and include flowing groundwater. However, since these Ra adsorption/desorption reactions are fast, it is useful to compare *in situ* sediment and groundwater Ra activities ratios to laboratory determined K_d values.

Several caveats need to be identified to compare K_ds from various laboratory experiments to *in situ* K_ds since it is possible to control variables in experimental determinations of K_d, but in the field, sediment characteristics, salinity and groundwater redox potential all vary simultaneously. One major difference with the laboratory experiments is the high water to sediment ratio (~5-30), resulting in an operationally defined K_d (based on the volume of water mixed with the sediment) that may be different than that expected in nature (Benes, 1990). It is also important to determine which fraction of the sedimentary Ra pool is being used to calculate K_d. In some instances, bulk sediment Ra is used, in others some operationally defined "exchangeable" fraction is used, the rationale being that Ra within the crystalline lattice of the sediment is not readily exchangeable with pore waters (Puigdomènech and Bergström, 1995). This can, however, result in greatly differing K_d values. In this study, we use surface bound ^{226}Ra to determine K_d. Pore water ^{226}Ra collected from the same locations as our sediment core (shaded regions, Figure 2c) allow us to reconstruct the *in situ* K_d.

The desorption experiment K_d varies from 210 to 475, and decreases with increasing salinity (Table 3, Figure 7a). However, this relationship varies depending on the sediment type. The K_d decrease, for all three sediments, from salinity 5 to 25 is 16-40%. The salinity/ K_d relationship averaged over the 48 hour desorption experiment (n=6) can be described by a linear fit to the data:

2) $K_d = -2.8 \times \text{salinity} + 270$ (Top), $r^2 = 0.28$

3) $K_d = -2.8 \times \text{salinity} + 490$ (Middle), $r^2 = 0.05$

4) K_d = -9.5 x salinity + 460 (Bottom), r^2 = 0.57

The presence of Mn and Fe (hydr)oxides also has a great impact on K_d. Ra was strongly bound to sediments with greater amounts of Mn and Fe (hydr)oxides (Figures 7b and 7c). When plotted against sediment Mn and Fe (hydr)oxide content, there is a increase in K_d with increasing Mn and Fe (hydr)oxide content (Figure 7b and 7c). However, the relationship between Mn (hydr)oxide content and K_d varies by sediment type, with Mn curtain sediments having a lower than anticipated K_d, likely due to the dissolution of Mn (hydr)oxides containing large amounts of ^{226}Ra within the desorption experiments (see discussion in Section 4.1 regarding the high surface bound ^{226}Ra).

Within the Waquoit STE, *in situ* ^{226}Ra K_ds vary from 90 to 1100 for the region where sediment for the above experiments was collected from (see shaded regions in Figure 2c). There is a decrease in K_d with increasing salinity, which is expected given the K_d:salinity relationship reported above (Figure 8a). Likewise, the *in situ* K_d also increases with increasing sedimentary Fe (hydr)oxide content (Figure 8c). The relationship between Mn (hydr)oxide content and K_d changes for the Mn curtain zone, similar to the experimental K_d (Figure 8b). The sediments from the "Mn curtain" have the lowest K_d, which is likely due to the dissolution of Mn (hydr)oxide, as evidence by low Eh and high pore water dissolved Mn, and subsequent release of radium within this reducing zone, as seen in Figure 2c. Thus, it seems that the relationship between the *in situ* K_d and sedimentary Mn (hydr)oxide content is driven by the pore water redox potential since it is the dissolution of the Mn (hydr)oxides, and subsequent release of Ra, that drives the pore water Ra activity at this depth. The dependence of K_d on sediment chemistry that we observe here highlights the importance of determining this relationship specifically for the STE sediments being studied. There is no one linear fit to the data since we are not capable of resolving the influence of salinity and redox conditions within the *in situ* data, thus complicating models of Ra desorption.

Previous estimates of the distribution coefficient for Ra range from 50 to 5000 (Puigdomènech and Bergström, 1995) (Table 4). Li and Chan (1979) reported a K_d of 235 for fine-grained Hudson Bay sediments. Webster et al. (1995) used a series of desorption experiments to construct a model of the effect of salinity on Ra desorption, and reported a K_d of 75 for fine-grained sediments. Rama and Moore (1996) reported a

very low K_d of 45 (converted from 10 L/cm^3) for fine-grained sediments from a salt marsh, and hypothesized that it was due to organic coating of the sediments, which neutralized the sorption capacity of the (Fe and Mn) mineral phases. The K_d values reported here from laboratory experiments, ranging from 210 to 475, are mostly higher than those reported for fine-grained sediments, as expected for permeable sands, but are in range with distribution coefficients of Ra in aquifers. The *in situ* K_ds display a greater range, from 90 to 1100, but also fall within the range of previously reported partitioning relationships.

5. Conclusions

The adsorption/desorption experiments reveal several important characteristics of Ra behavior during sediment-water interaction in coastal aquifers. First, the length of time sediments are in contact with water does not significantly increase the amount of long-lived Ra that desorbs, verifying the conclusion of Langmuir and Riese (1985) that Ra adsorption-desorption reactions "go to completion within seconds to a few hours." Given the time scales of flow in most aquifers, for modeling and other considerations, we can assume that groundwater radium is in equilibrium with the sediment. Exceptions may include short-term seawater intrusion events such as those due to tidal pumping. Second, increases in salinity result in greater Ra desorption, however the decrease in K_d associated with an increase in salinity varies depending on the chemical characteristics of the sediment. Third, pH does play a role in Ra desorption, with low pH favoring Ra release even at zero salinity, suggesting that this release is driven primarily by dissolution of Ra-containing oxides. Given the redox dynamics of the Waquoit STE, with low pH in relatively oxidizing regions, pH does not appear to be a main driver of Ra desorption. Fourth, sediments with greater amounts of Fe and Mn (hydr)oxides retain a greater proportion of Ra even when exposed to saline water, as is evident by the increase in K_d with increasing oxide content. In all, these sediments have a large capacity to sorb Ra, which is favored under low salinity conditions.

Because the STE sediments are in a dynamic setting with flowing groundwater, the in situ derived K_ds are only valid if equilibrium states are established very quickly. The disadvantage of the laboratory experiments on the other hand is that it is hard to

simulate *in situ* pore water to sediment ratios and redox potentials. Hence, it is encouraging that our conclusions were consistent between field and laboratory studies. The groundwater and sediment profiles within the Waquoit Bay STE indicate that salinity together with the Mn and Fe redox cycle all influence Ra partitioning. While radium has a much greater affinity for Mn (hydr)oxides than Fe (hydr)oxides, throughout much of the STE Fe (hydr)oxides are more abundant (sediment Fe/Mn ~ 40-300); both are therefore likely involved in controlling sediment-water Ra partitioning. Though Ra desorption by ion exchange is an important process, it is difficult to decouple its importance relative to Fe and Mn within the natural environment, as the redox state is largely driven by the influx of organic matter carried by circulating seawater. Though salinity may be less effective than Fe and Mn redox chemistry at controlling Ra cycling in coastal groundwater systems, one must put into perspective the relative areas and concentrations over which these processes are at work in the STE. In our site, they appear to be about equal but this may not be true in other STEs, given the large Fe and Mn (hydr)oxide content and vertical extent of the Waquoit aquifer sands. Ideally, our results would allow one to predict coastal groundwater Ra activities given the salinity of the pore water and the oxide content of the sediment. However, the interplay between salinity and redox conditions on Ra cycling in our STE prevents us from extending our results to other settings using a simple model.

Given these findings, we recommend that future studies using Ra to derive SGD consider the following: 1) Ra activities should be measured across the full extent of the salinity range present in the groundwater. For example, we observed Ra values at salinities of 1 and 25 that had the same activity–an unexpected result given what we know about Ra cycling in surface estuaries. In addition, at salinities <1, we observed measurable radium, hence even "fresh" groundwater may be a source of radium to surface waters, especially when fresh groundwater represents a significant portion of total SGD (as in Mulligan and Charette, 2006). 2) Measure the groundwater and (if possible) sediment Mn and Fe content to determine if active cycling of these elements is present within the STE, since they influence Ra cycling. In the absence of Fe and Mn concentrations, groundwater redox potential (Eh and pH as measured by a YSI electrode or the equivalent) will provide useful information about the potential for active Fe and

Mn redox cycling to be occurring. 3) If possible, determine exchangeable Ra inventories for sediment throughout the STE, since as we observed here, this value can vary considerably, even when bulk Ra shows little change. We recommend a simple approach for determining this quantity using ^{222}Rn equilibration. 4) We observed seasonality in radium release within these sediments, thus measurements of groundwater radium activities collected in one season may not be applicable to all seasons; groundwater radium activities should be determined concurrently with surface water measurements. Such measures should help insure the most appropriate groundwater radium activity is used, which will in turn minimize uncertainty in quantifying SGD to the coastal ocean.

Acknowledgements

The authors thank Paul Henderson, Gillian Smith, DeAnna McCadney and Grace Rago for assistance in the field and laboratory. David Schneider of the WHOI ICP-MS Facility performed the trace metal analyses. We extend our continued appreciation to the director and staff of the Waquoit Bay National Estuarine Research Reserve for their assistance with logistics during field sampling. This work is a result of research sponsored by NSF (OCE- 0425061 to M.A.C.), the WHOI-NOC Student Exchange program (to P.J.M), and the WHOI Postdoctoral Scholar program (to H.D.). We would like to thank two anonymous reviewers and guest editor Jan Scholten for comments that led to improvements with the manuscript.

References

Abraham, D.M., Charette, M.A., Allen, M.C., Rago, A. and Kroeger, K.D., 2003. Radiochemical estimates of submarine groundwater discharge to Waquoit Bay, Massachusetts. Biol. Bull., 205:246-247.

Benes, P., 1990. Radium in continental surface water. In: IAEA Technical Report Series No. 310, The Environmental Behaviour of Radium, 1:373-418.

Bollinger, M.S. and Moore, W.S., 1993. Evaluation of salt marsh hydrology using radium as a tracer. Geochim. Cosmochim. Acta, 57:2203-2212.

Bone, S.E., Gonneea, M.E. and Charette, M.A., 2006. Geochemical cycling of arsenic in a coastal aquifer. Environ. Sci. Technol., 40:3273-3278.

Burnett, W.C., Coward, J.B, and Deetae, S. 1990. Radium in the Suwannee River and estuary. Biogeochem. 10:237-255.

Burnett, W.C., P.K. Aggarwal, A. Aureli, H. Bokuniewicz, J.E. Cable, M.A. Charette, E. Kontar, S. Krupa, K.M. Kulkarni, A. Loveless, W.S. Moore, J.A. Oberdorfer, J. Oliveira, N. Ozyurt, P. Povinec, A.M.G. Privitera, R. Rajar, R.T. Ramessur, J. Scholten, T. Stieglitz, M. Taniguchi, J.V. Turner, 2006. Quantifying submarine groundwater discharge in the coastal zone via multiple methods. Sci. Total Environ., 367:498-543.

Cambareri, T.C., and Eichner, E.M., 1998. Watershed delineation and ground water discharge to a coastal embayment. Ground Water, 36:626-634.

Charette, M.A., Buesseler, K.O. and Andrews, J.E., 2001. Utility of radium isotopes for evaluating the input and transport of groundwater-derived nitrogen to a Cape Cod estuary. Limnol. Oceanogr., 46:465-470.

Charette, M.A. and Sholkovitz, E.R., 2002. Oxidative precipitation of groundwater-derived ferrous iron in the subterranean estuary of a coastal bay. Geophys. Res. Lett., 29:1444-1447, doi: 10.1029/2001GL014512.

Charette, M.A., Splivallo, R., Herbold, C., Bollinger, M. and Moore, W.S., 2003. Salt marsh submarine groundwater discharge as traced by radium isotopes, *Marine Chemistry*, 84:113-121.

Charette, M.A., Sholkovitz, E.R. and Hansel, C., 2005. Trace element cycling in a subterranean estuary: Part 1. Geochemistry of the permeable sediments. Geochim. Cosmochim. Acta, 69:2095-2109.

Charette, M.A., and Allen, M.C., 2006. Precision ground water sampling in coastal aquifers using a direct-push, shielded-screen well-point system. Ground Water Monit. R., 26(2):87-93.

Charette, M.A., 2007. Hydrologic forcing of submarine groundwater discharge: Insight from a seasonal study of radium isotopes in a groundwater-dominated salt marsh estuary. Limnol. Oceanogr., 52:230.

Charette, M.A. and Shokovitz, E.R., 2006. Trace element cycling in a subterranean eastury: Part 2. Geochemistry of the pore water. Geochim. Cosmochim. Acta, 70:811-826.

Corrbett, D. R., W. C. Burnett, P. H. Cable, and S. B. Clark, 1998. A multiple approach to the determination of radon fluxes from sediments. J. Radioanal. Nucl. Ch. 236: 247-252.

De Geer, L. (2004) Currie detection limits in gamma-ray spectroscopy. Appl. Radiat. Isotopes, 61:151-160.

Elsinger, R.J. and Moore, W.S., 1980. ^{226}Ra behavior in the Pee Dee River-Winyah Bay Estuary. Earth Planet. Sc. Lett., 48:239-249.

Gonneea, M. E., Mulligan, A. and Charette, M. A., 2006. Seasonal trends in radium activities within the mixing zone of a subterranean estuary, Waquoit Bay, MA. Eos Transactions AGU Ocean Sciences Meeting Supplement, 87(36), Abstract OS15B-01.

Grundl, T. and Cape, M., 2006. Geochemical factors controlling radium activity in a sandstone aquifer. Groundwater, 44:518-527.

Hall, G.E.M., Vaive, J.E, Beer, R. and Hoashi, M., 1996. Selective leaches revisited, with emphasis on the amorphous Fe oxyhydroxide phase extraction. J. Geochem. Explor., 56:59-78.

Hancock, G. J., Webster, I. T. and Stieglitz, T. C., 2006. Horizontal mixing of Great Barrier Reef waters: Offshore diffusivity determined from radium isotope distribution, J. Geophys. Res., 111:C12019, doi:10.1029/2006JC003608.

Kelly, R.P. and Moran S.B., 2002. Seasonal changes in groundwater input to a well-mixed estuary estimated using radium isotopes and implications for coastal nutrient budgets. Limnol. Oceanogr., 47:1796-1807.

Koulouris, G., 1995. Dynamic studies on sorption characteristics of ^{226}Ra on manganese dioxide. J. Radioan. Nucl. Ch. Ar., 193:269-279.

Langmuir, D. and Riese, A.C., 1985. The thermodynamic properties of radium. Geochim. Cosmochim. Acta, 49:1593-1601.

Lauria, D.C., Almeida, R.M.R., and Sracek, O. 2004. Behavior of radium, thorium and uranium in groundwater near the Buena Lagoon in the coastal zone of the state of Rio de Janeiro, Brazil. Environ. Geol. 47:11-19.

Li, Y. and Chan, L., 1979. Desorption of Ba and ^{226}Ra from river-borne sediments in the Hudson estuary. Earth Planet. Sc. Lett., 43:343-350.

Martin, P., Hancock, G.J., Paulka, S. and Akber, R.A., 1995. Determination of 227Ac by α–particle spectrometry. Appl. Radiat. Isot. 46:1065-1070.

Miao, S, DeLaune, R.D. and Jugsujinda, A., 2006. Influence of sediment redox conditions on release/solubility of metals and nutrients in a Louisiana Mississippi River deltaic plain freshwater lake. Sci. Total Environ., 371:334-343.

Michael, H.A., Mulligan, A.E. and Harvey, C.F., 2005. Seasonal oscillations in water exchange between aquifers and the coastal ocean. Nature, 436:1145-1148.

Moore, W.S., and Reid, D.F., 1973. Extraction of radium from natural waters using manganese-impregnated acrylic fibers. J. Geophys. Res., 78: 8880-8886.

Moore, W.S., and Arnold, R., 1996. Measurement of ^{223}Ra and ^{224}Ra in coastal water using a delayed coincidence counter. J. Geophys. Res., 101: 1321-1329.

Moore, W.S. 1997. High fluxes of radium and barium from the mouth of the Ganges-Brahmaputra River during low river discharge suggest a large groundwater source. Earth Planet. Sc. Lett., 150:141-150.

Moore, W.S., 1999. The subterranean estuary: a reaction zone of ground water and sea water. Mar. Chem., 65:111-125.

Mulligan, A.E., and Charette, M.A., 2006. Intercomparison of submarine groundwater discharge estimates from a sandy unconfined aquifer. J. Hydrol., 327:411-425.

Porcelli, D. and Swarzenski, P.W., 2003. The behaviour of U- and Th-series nuclides in groundwater. Rev. Mineral. Geochem., 52:317-361.

Puigdomènech and Bergström, U., 1995. Calculation of distribution coefficients for radionuclides in soils and sediments. Nucl. Safety, 36:142-154.

Rama and Moore, W.S., 1996. Using the radium quartet for evaluating groundwater input and water exchange in salt marshes. Geochim. Cosmochim. Acta, 60:4645-4652.

Sanchez, F. and Rodriguez-Alvarez, M.J. 1999. Effect of pH, conductivity, temperature and sediment size on thorium and radium activities along Jucar River (Spain). J. Radioanal. Nucl. Ch., 242:671-681.

Shellenbarger, G.G., Monismith, S.G., Genin, A. and Paytan, A., 2006. The importance of submarine groundwater discharge to the nearshore nutrient supply in the Gulf of Aqaba (Israel). Limnol. Oceanogr., 51:1876.

Sima O. and Arnold, D. 2002. Transfer of the efficiency calibration of Germanium gamma-ray detectors using the GESPECOR software. Appl. Radiat. Isotopes, 56:71-75.

Slomp, C.P. and van Cappellan, P., 2004. Nutrient inputs to the coastal ocean through submarine groundwater discharge: controls and potential impact. J. of Hydrol., 295: 64-86.

Sun, Y. and Torgersen, T., 1998. The effects of water content and Mn-fiber surface conditions on Ra-224 measurement by Rn-220 emanation. Mar. Chem. 62:299-306.

Sun, Y. and Torgersen, T., 2001. Adsorption-desorption reactions and bioturbation transport of ^{224}Ra in marine sediments: a one-dimensional model with applications. Mar. Chem., 74:227-243.

Talbot, J.M., Kroeger, K.D., Rago, A., Allen, M.C. and Charette, M.A., 2003. Nitrogen flux and speciation through the subterranean estuary of Waquoit Bay, Massachusetts. Biol. Bull. 205:244-245.

Testa, J.M., Charette, M.A., Sholkovitz, E.R., Allen, M.C., Rago, A. and Herbold, C.W., 2002. Dissolved iron cycling in the subterranean estuary of a coastal bay: Waquoit Bay, Massachusetts. Biol. Bull. 203:255-256.

Tricca, A., Wasserburg, G.J., Porcell, D. and Baskaran, M., 2001. The transport of U- and Th-series nuclides in a sandy unconfined aquifer. Geochim. Cosmochim. Acta, 65:1187-1210.

Valiela, I., Costa, J., Foreman, K., Teal, J.M., Howes, B. and Aubrey D., 1990. Transport of Groundwater-Borne Nutrients from Watersheds and Their Effects on Coastal Waters. Biogeochem., 10:177-197.

Webster, I.T., Hancock, G.J., and Murray, A.S., 1995. Modeling the effect of salinity on radium desorption from sediments. Geochim. Cosmochim. Acta, 59:2469-2476.

Windom, H. and Niencheski, F. 2003. Biogeochemical processes in a freshwater-seawater mixing zone in permeable sediments along the coast of Southern Brazil. Mar. Chem., 83:121-130.

Table 1. Desorption/adsorption experiment sediment characteristics.

Sediment	Sediment Fe^{2} µmol/kg	Sediment Mn^{2} µmol/kg	Total ^{226}Ra dpm/100g	Surface bound $^{226}Ra^{1}$ dpm/100g	% Surface bound ^{226}Ra of bulk ^{226}Ra	Total ^{228}Ra dpm/100g	Sediment $^{228}Ra/^{226}Ra$
Top PZ 11, 2.1-3.1 m	13000	45	32 ± 1.1	6 ± 0.5 (n=2)	19%	53 ± 2.8	1.66
Middle, PZ 11, 4.6-5.6 m	43000	1170	38 ± 1.2	10 ± 1.5 (n=2)	26%	44 ± 3.1	1.14
Bottom, PZ 11, 5.8-6.5 m	8700	2500	46 ± 1.3	32 ± 1.6 (n=2)	70%	42 ± 2.8	0.90

[1]Surface bound ^{226}Ra was determined via radon emanation after the sediment had equilibrated with salinity 10.8 water (Section 2.4).
[2]Exchageable Fe and Mn (hydr)oxides determined by leaching sediment in 0.25 M hydroxylamine hydrochloride in 25% glacial acetic acid and heated for 3 hours at 90° (Section 2.3).

Table 2. Ra desorption at salinity 5, 15 and 25 for sediments from PZ11. Each value represents the average of six time points during the 48 hour experiment.			
Sediment	**^{226}Ra dpm/100g**	**^{228}Ra dpm/100g**	**228/226**
Top PZ 11, (Intermed. Fe, Low Mn)			
Salinity 5	0.36 ± 0.09	4.8 ± 0.44	13
Salinity 15	0.46 ± 0.05	6.9 ± 0.81	15
Salinity 25	0.48 ± 0.06	6.9 ± 0.71	13
Middle, PZ 11, (High Fe, Intermed. Mn)			
Salinity 5	0.36 ± 0.06	0.35 ± 0.31	0.97
Salinity 15	0.36 ± 0.05	0.65 ± 0.17	1.8
Salinity 25	0.42 ± 0.11	0.81 ± 0.23	1.9
Bottom, PZ 11, (Low Fe, High Mn)			
Salinity 5	1.2 ± 0.43	0.41 ± 0.29	0.33
Salinity 15	1.4 ± 0.08	0.55 ± 0.10	0.38
Salinity 25	2.1 ± 0.42	0.74 ± 0.19	0.35

Table 3. K_d (L/Kg) for the desorption experiments at salinity 5, 15 and 25 calculated from surface bound ^{226}Ra. Each value represents the average of six time points during the 48 hour experiment.			
Salinity	**Top PZ 11, 2.1-3.1 m**	**Middle, PZ 11, 4.6-5.6 m**	**Bottom, PZ 11, 5.8-6.5 m**
5	270 ± 50	475 ± 90	408 ± 115
15	210 ± 25	445 ± 100	330 ± 25
25	210 ± 40	420 ± 120	220 ± 30

Table 4. Radium K_d (L/Kg) in natural sediments.		
Aquifers	50 to 5000	Puigdomènech and Bergström (1995)
Fine-grained sediment Saline/fresh	235/21,000	Li and Chan (1979)
Fine-grained sediment	75	Webster et al. (1995)
Fine-grained sediment	45	Rama and Moore (1996)
Permeable sands	210-475*	This Study

*Desorption experiment data only.

Figure Captions

Figure 1: Map of the study area including a cross section of the Waquoit Bay subterranean estuary. The salinity transition zone (STZ) is indicated with a dashed line. The location of sediment and groundwater samples is marked by PZ 7, 6 and 11. Time series data originated from the TS profile. The shaded region indicates where sediment for the adsorption/desorption experiments was collected.

Figure 2: Groundwater profiles of salinity, Eh, pH, ^{226}Ra, ^{228}Ra, Ba, Mn and Fe and sediment Mn and Fe for a) PZ 7, b) PZ 6 and c) PZ 11. Shaded regions in (c) indicate the depth range from which sediments for the adsorption/desorption experiments were collected.

Figure 3: Desorbed ^{226}Ra from PZ 11 (a) top, (b) middle, and (c) bottom and ^{228}Ra from PZ 11 (d) top, (e) middle, and (f) bottom at salinity 5 (empty squares), 15 (black triangles) and 25 (grey circles). Error bars represent analytical uncertainties.

Figure 4: Desorption from a) top, b) middle and c) bottom sediments at pH 5 (black) and 8 (grey) for salinity 0, 5 and 25. Note these sediments were spiked with ^{226}Ra prior to desorption (see methods section for details). Error bars represent analytical uncertainties.

Figure 5: ^{226}Ra adsorption capacity of PZ 11 sediments from the top (diamonds), middle (squares) and bottom (triangles) versus salinity. Error bars are plotted for all data but are smaller than the symbol in some cases.

Figure 6: Time series measurements at 3.4 m (open symbols) and 4.7 m (filled symbols) within the Waquoit Bay STE of salinity, Eh, pH, ^{226}Ra, dissolved Mn and dissolved Ba. Note the different scales for the parameters between the two depths.

Figure 7: Experimental distribution coefficients (K_d) plotted against a) salinity, b) sediment Mn (hydr)oxides and c) Fe (hydr)oxides. Data is the average of six time points during the 48 hour desorption experiment, and b) and c) contain data only from salinity 25. The linear fits between K_d and salinity in a) are represented by the dotted line (top, $r^2 = 0.28$), dashed line (middle, $r^2 = 0.05$) and solid line (bottom, $r^2 = 0.57$). Error bars represent the standard deviation of six K_d values.

Figure 8: *In situ* ^{226}Ra K_ds plotted against a) salinity, b) sediment Mn (hydr)oxides and c) Fe (hydr)oxides. Error bars represent analytical uncertainties.

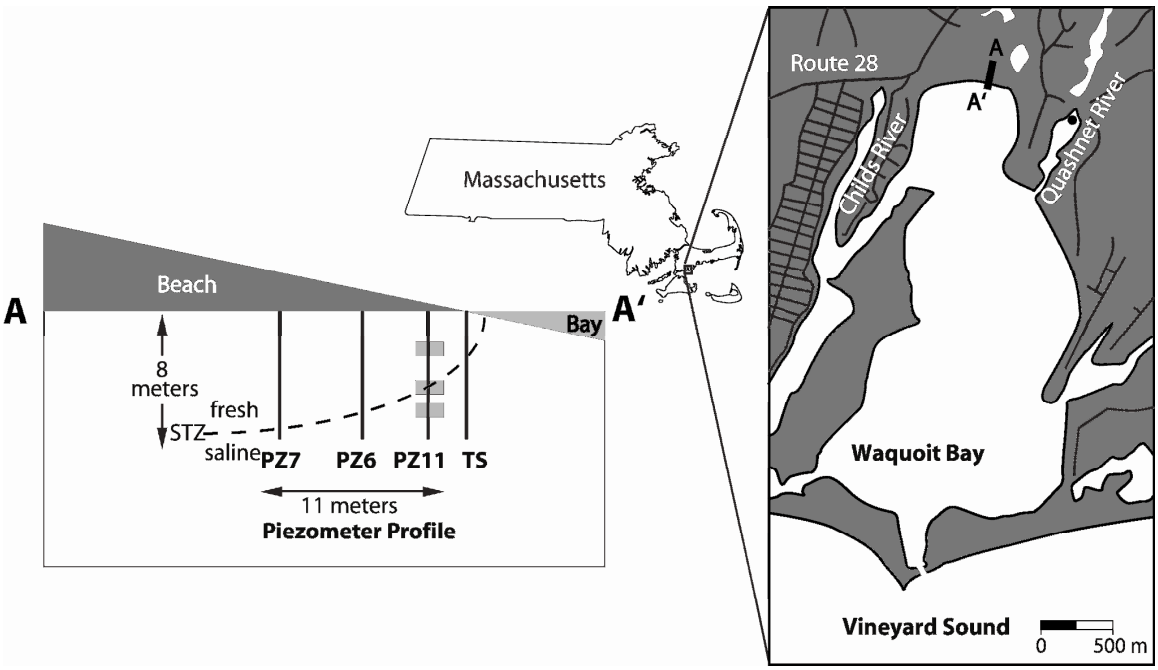
Massachusetts
A
A′
Beach
Bay
8
meters
fresh
STZ
saline
PZ7
PZ6
PZ11
TS
11 meters
Piezometer Profile
Route 28
A
A′
Childs River
Quashnet River
Waquoit Bay
Vineyard Sound
0
500 m

Figure 1

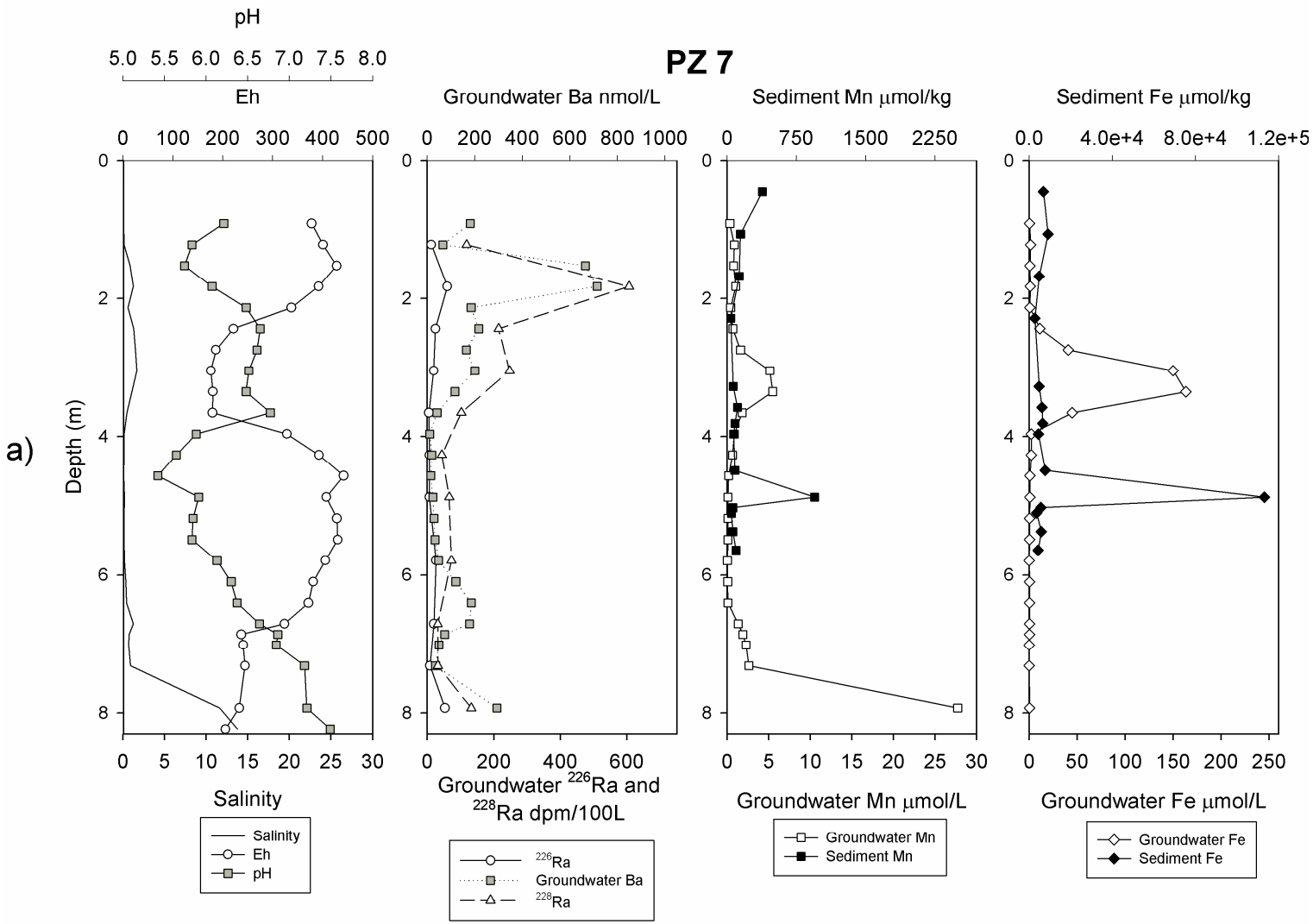
PZ 7
a)
pH
5.0 5.5 6.0 6.5 7.0 7.5 8.0
Eh
0 100 200 300 400 500
Depth (m)
0 2 4 6 8
0 5 10 15 20 25 30
Salinity
Salinity
Eh
pH
Groundwater Ba nmol/L
0 200 400 600 800 1000
0 200 400 600
Groundwater 226Ra and 228Ra dpm/100L
226Ra
Groundwater Ba
228Ra
Sediment Mn μmol/kg
0 750 1500 2250
0 5 10 15 20 25 30
Groundwater Mn μmol/L
Groundwater Mn
Sediment Mn
Sediment Fe μmol/kg
0.0 4.0e+4 8.0e+4 1.2e+5
0 50 100 150 200 250
Groundwater Fe μmol/L
Groundwater Fe
Sediment Fe

Figure 2a

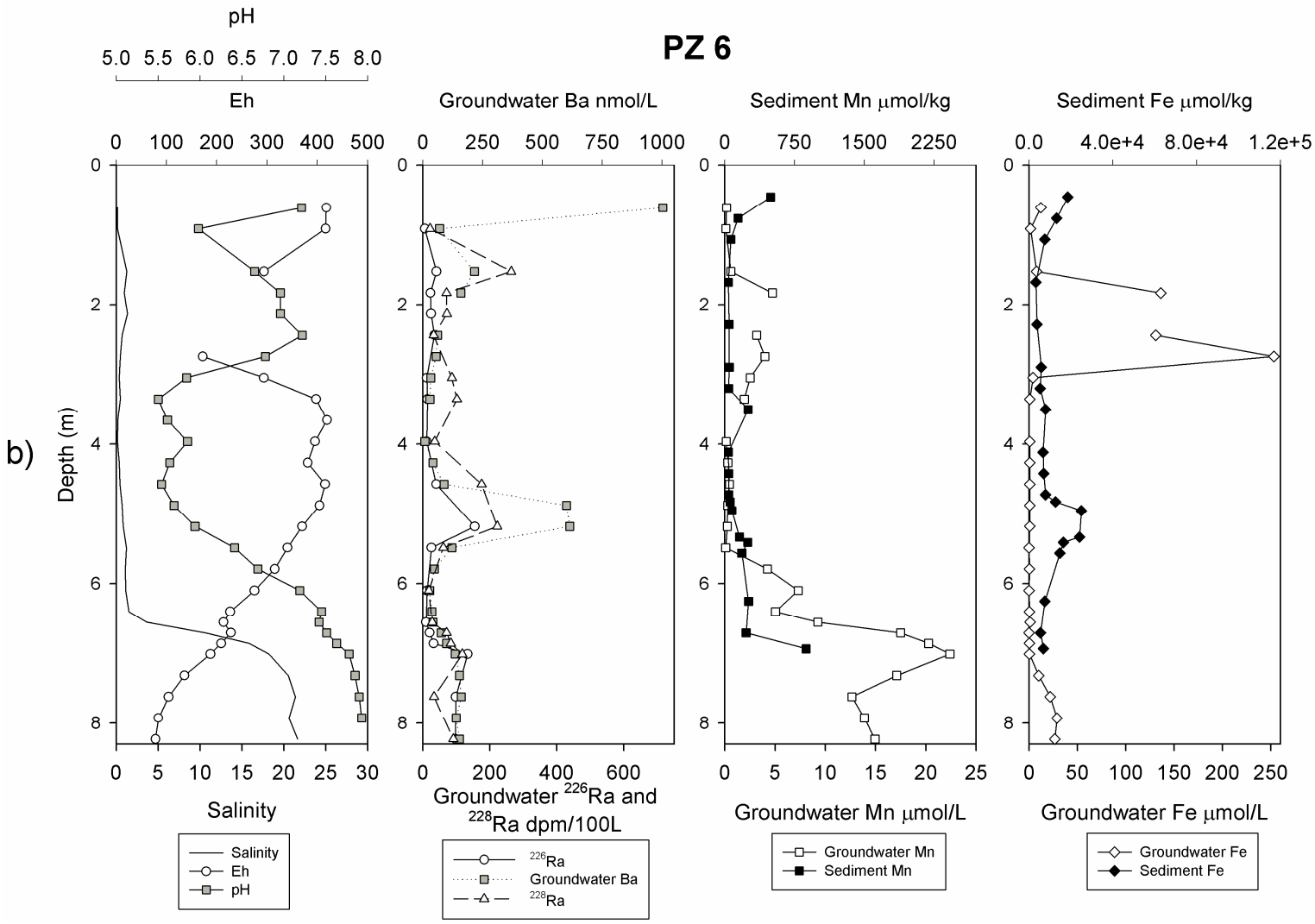
b)
PZ 6
pH
5.0 5.5 6.0 6.5 7.0 7.5 8.0
Eh
0 100 200 300 400 500
Depth (m)
0 2 4 6 8
0 5 10 15 20 25 30
Salinity
Salinity
Eh
pH
Groundwater Ba nmol/L
0 250 500 750 1000
0 200 400 600
Groundwater 226Ra and 228Ra dpm/100L
226Ra
Groundwater Ba
228Ra
Sediment Mn μmol/kg
0 750 1500 2250
0 5 10 15 20 25
Groundwater Mn μmol/L
Groundwater Mn
Sediment Mn
Sediment Fe μmol/kg
0.0 4.0e+4 8.0e+4 1.2e+5
0 50 100 150 200 250
Groundwater Fe μmol/L
Groundwater Fe
Sediment Fe

Figure 2b

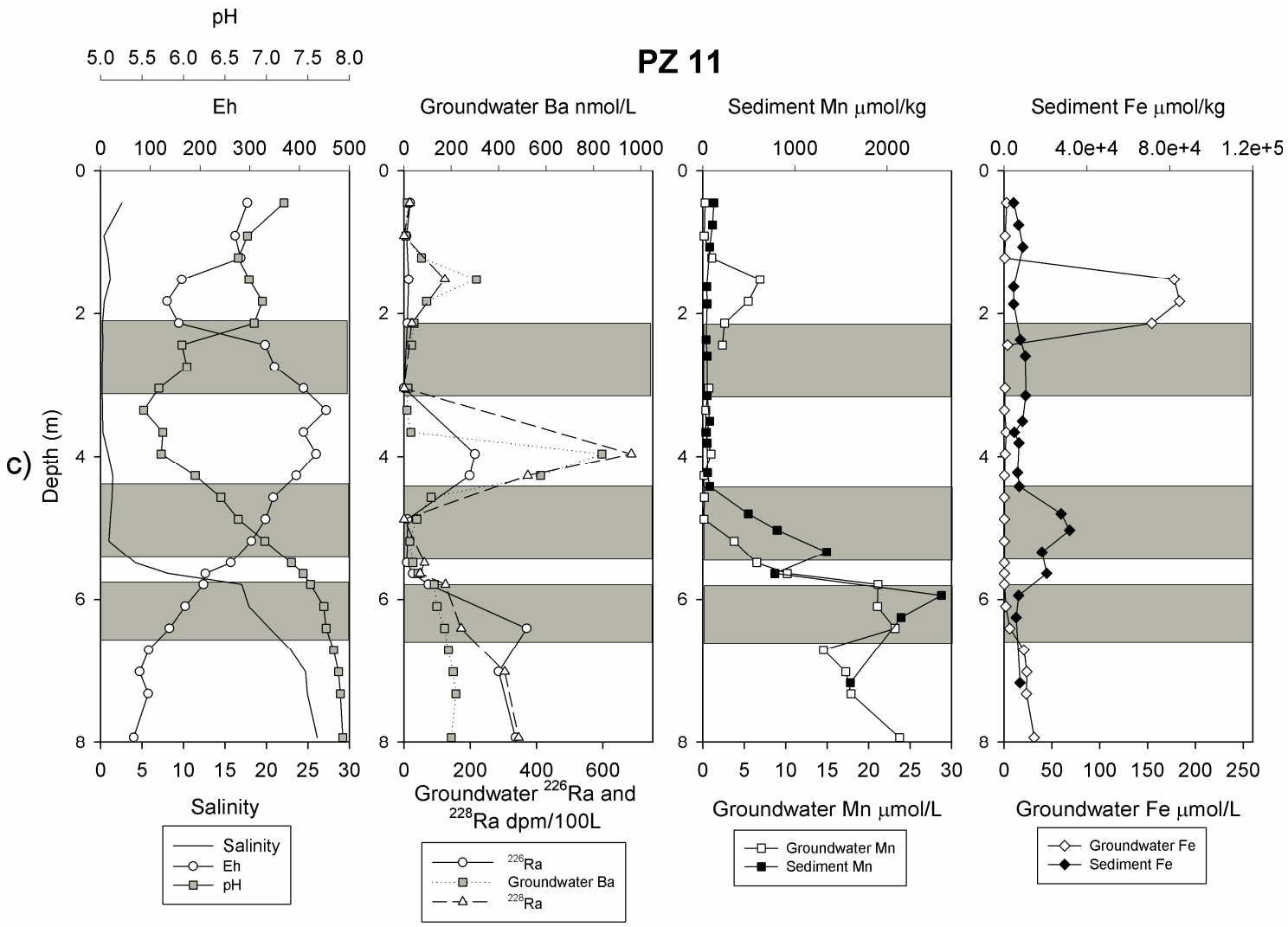
PZ 11
c)
pH
5.0 5.5 6.0 6.5 7.0 7.5 8.0
Eh
0 100 200 300 400 500
Depth (m)
Salinity
0 5 10 15 20 25 30
Salinity
Eh
pH
Groundwater Ba nmol/L
0 200 400 600 800 1000
Groundwater ^{226}Ra and ^{228}Ra dpm/100L
0 200 400 600
^{226}Ra
Groundwater Ba
^{228}Ra
Sediment Mn μmol/kg
0 1000 2000
Groundwater Mn μmol/L
0 5 10 15 20 25 30
Groundwater Mn
Sediment Mn
Sediment Fe μmol/kg
0.0 4.0e+4 8.0e+4 1.2e+5
Groundwater Fe μmol/L
0 50 100 150 200 250
Groundwater Fe
Sediment Fe

Figure 2c

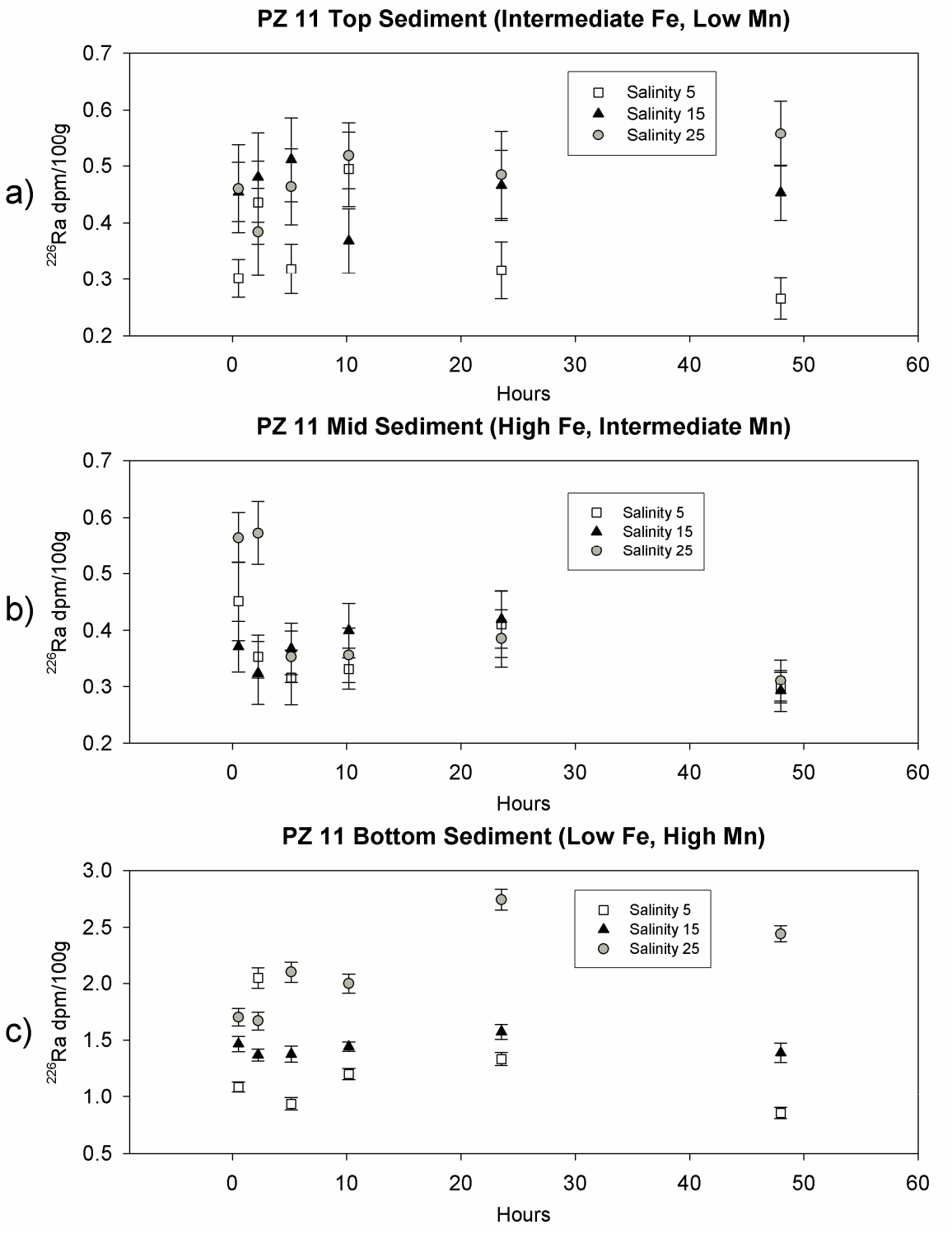
PZ 11 Top Sediment (Intermediate Fe, Low Mn)
a)
^{226}Ra dpm/100g
0.7
0.6
0.5
0.4
0.3
0.2
0
10
20
30
40
50
60
Hours
Salinity 5
Salinity 15
Salinity 25
PZ 11 Mid Sediment (High Fe, Intermediate Mn)
b)
^{226}Ra dpm/100g
0.7
0.6
0.5
0.4
0.3
0.2
0
10
20
30
40
50
60
Hours
Salinity 5
Salinity 15
Salinity 25
PZ 11 Bottom Sediment (Low Fe, High Mn)
c)
^{226}Ra dpm/100g
3.0
2.5
2.0
1.5
1.0
0.5
0
10
20
30
40
50
60
Hours
Salinity 5
Salinity 15
Salinity 25

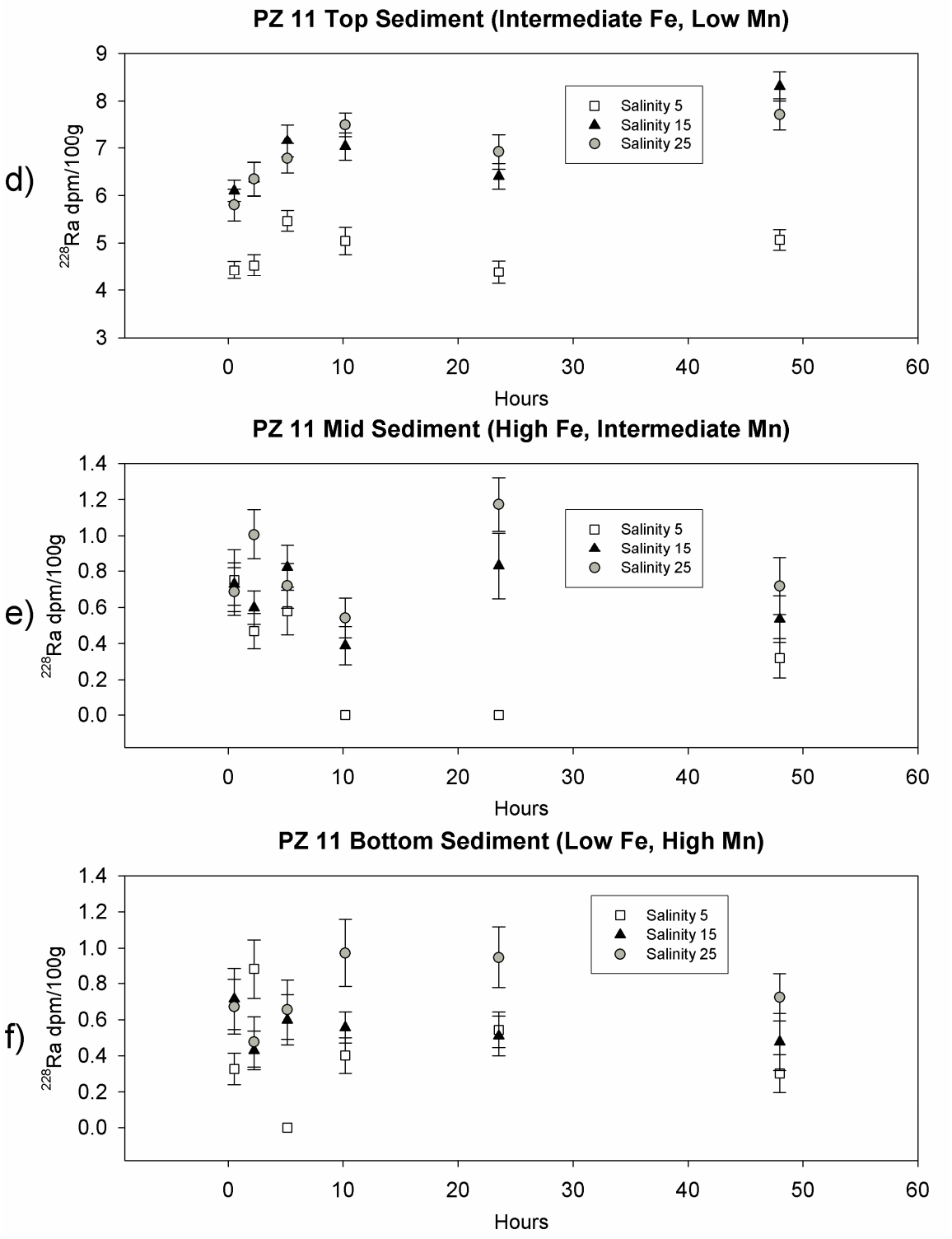
PZ 11 Top Sediment (Intermediate Fe, Low Mn)
d)
^{228}Ra dpm/100g
Salinity 5
Salinity 15
Salinity 25
Hours
PZ 11 Mid Sediment (High Fe, Intermediate Mn)
e)
^{228}Ra dpm/100g
Salinity 5
Salinity 15
Salinity 25
Hours
PZ 11 Bottom Sediment (Low Fe, High Mn)
f)
^{228}Ra dpm/100g
Salinity 5
Salinity 15
Salinity 25
Hours

Figure 3

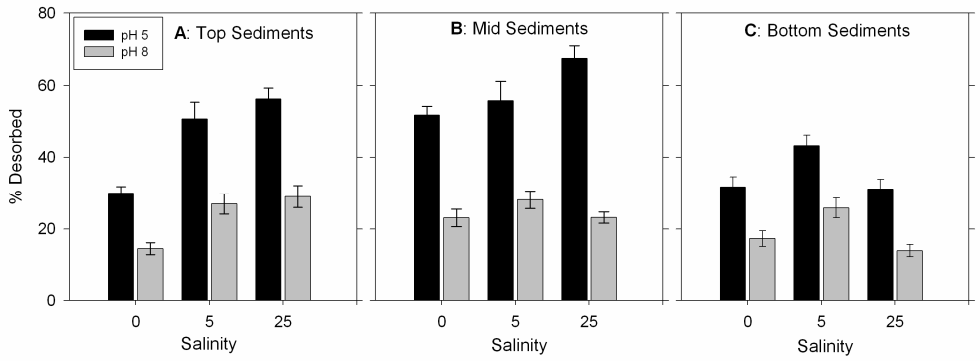
pH 5
pH 8
A: Top Sediments
B: Mid Sediments
C: Bottom Sediments
% Desorbed
80
60
40
20
0
0
5
25
Salinity

Figure 4

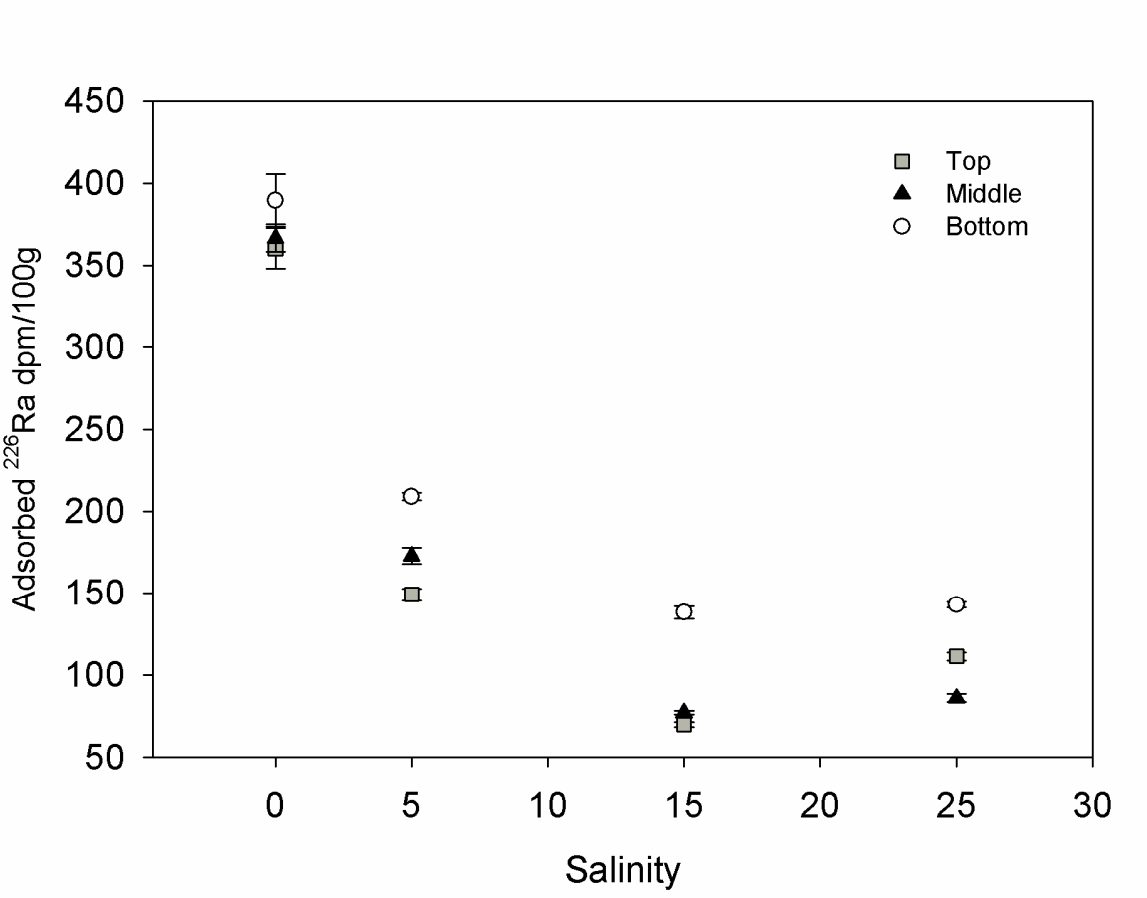
450
400
350
300
250
200
150
100
50
Adsorbed ^{226}Ra dpm/100g
0
5
10
15
20
25
30
Salinity
Top
Middle
Bottom

Figure 5

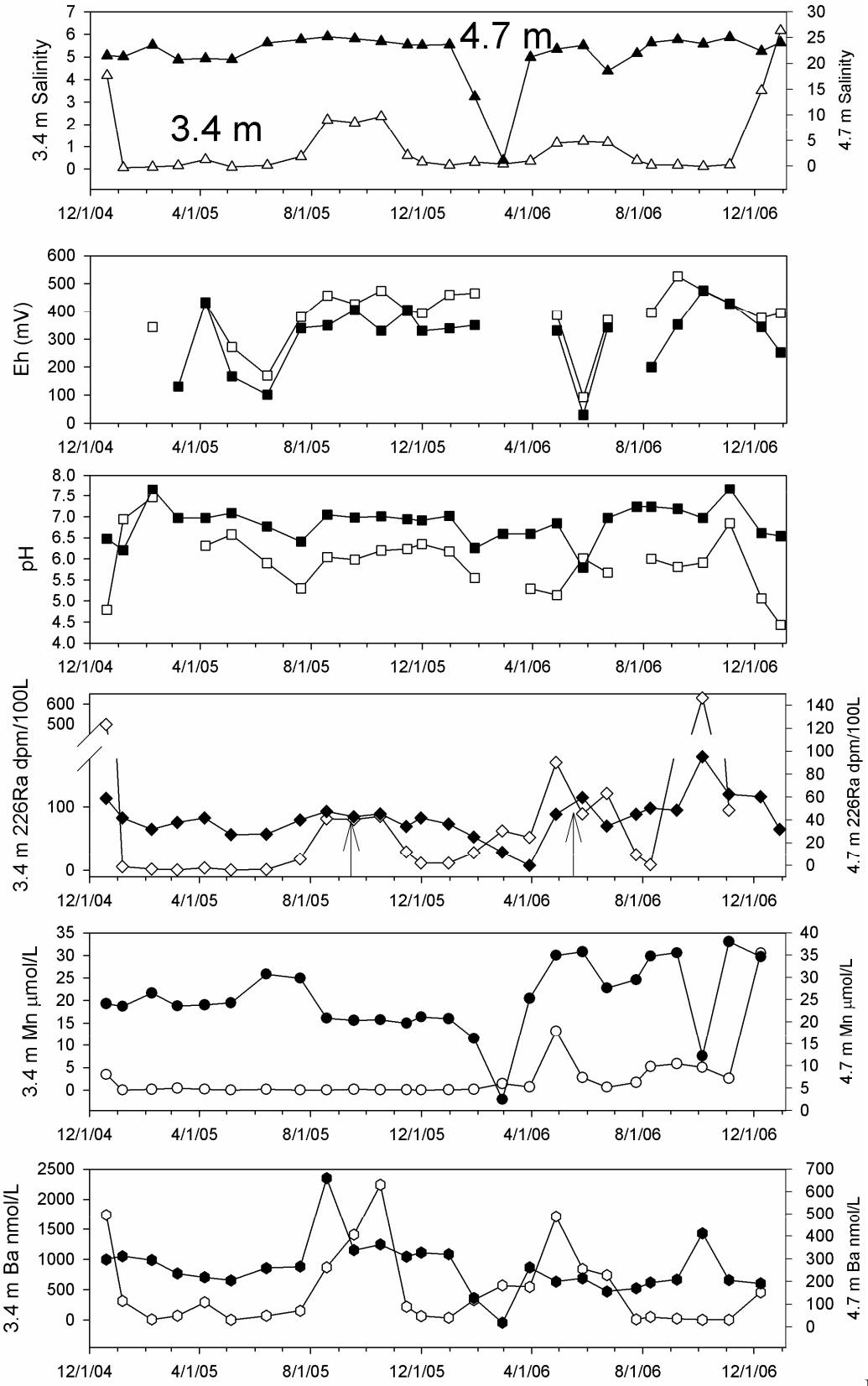
4.7 m
3.4 m
3.4 m Salinity
4.7 m Salinity
Eh (mV)
pH
3.4 m 226Ra dpm/100L
4.7 m 226Ra dpm/100L
3.4 m Mn µmol/L
4.7 m Mn µmol/L
3.4 m Ba nmol/L
4.7 m Ba nmol/L
12/1/04
4/1/05
8/1/05
12/1/05
4/1/06
8/1/06
12/1/06

Figure 6

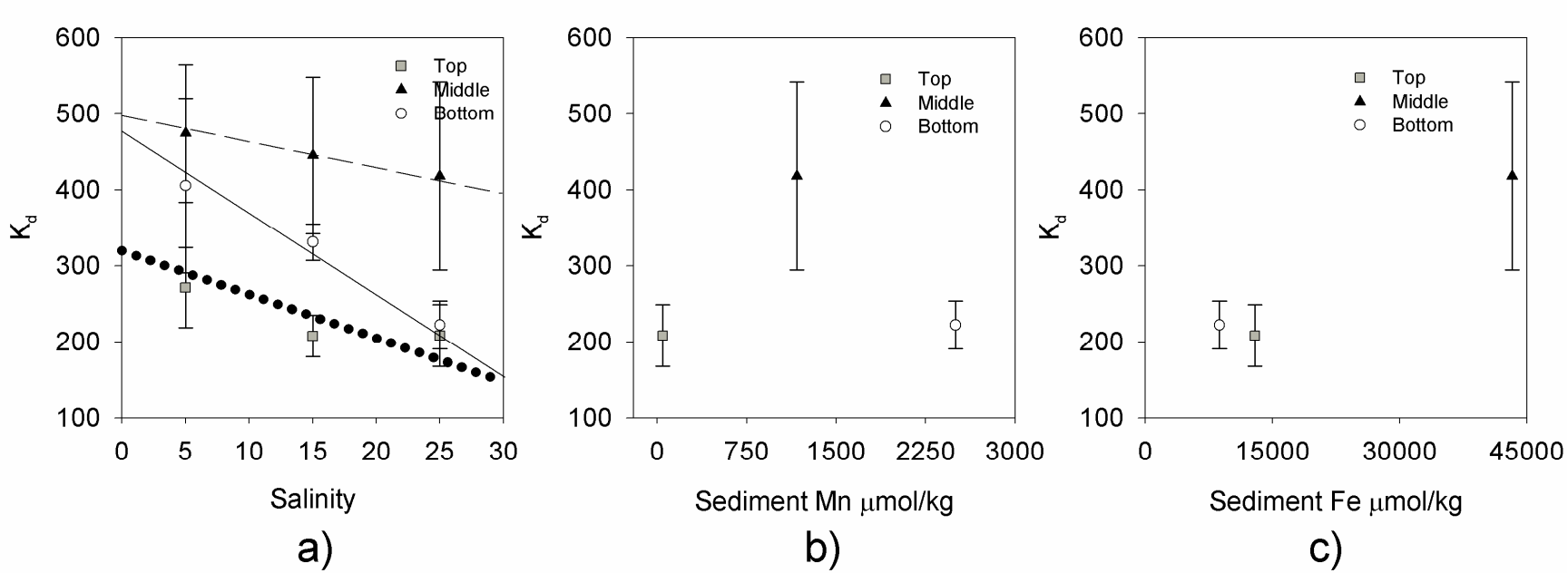
600
500
400
300
200
100
K_d
Top
Middle
Bottom
0
5
10
15
20
25
30
Salinity
a)
0
750
1500
2250
3000
Sediment Mn μmol/kg
b)
0
15000
30000
45000
Sediment Fe μmol/kg
c)

Figure 7 a-c

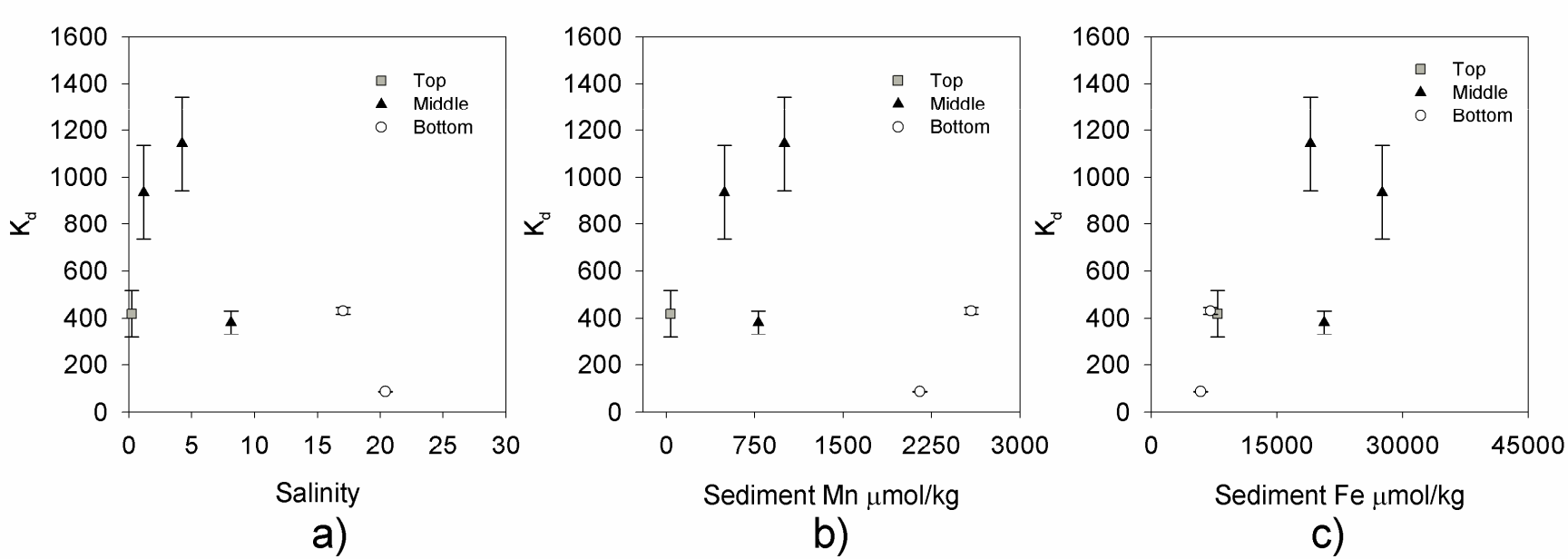
1600
1400
1200
1000
800
600
400
200
0
K_d
Top
Middle
Bottom
0 5 10 15 20 25 30
Salinity
a)
0 750 1500 2250 3000
Sediment Mn μmol/kg
b)
0 15000 30000 45000
Sediment Fe μmol/kg
c)

Figure 8 a-c